J. Fluid Mech. (2022), *vol*. 947, A12, doi:10.1017/jfm.2022.642

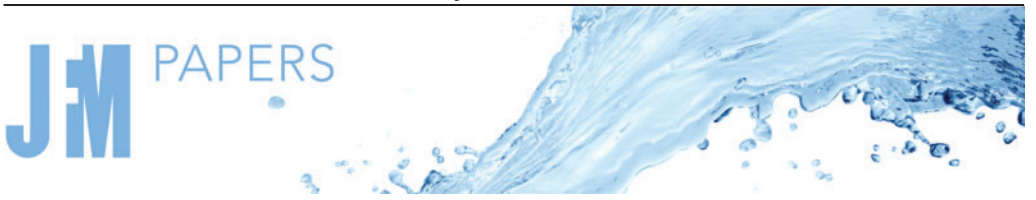

Investigation of the imbibition/drainage of two immiscible fluids in capillaries with arbitrary axisymmetric cross-sections: a generalized model

Amgad Salama†

Process System Engineering, Faculty of Engineering and Applied Science, University of Regina, Regina, SK S4S 0A2, Canada

(Received 20 January 2022; revised 9 June 2022; accepted 20 July 2022)

In this work, we investigate the problem of imbibition/drainage of a fluid in capillaries of arbitrary axisymmetric cross-sections filled initially with another immiscible one. The model predicts the location of the meniscus and its speed along the tube length with time. The two immiscible fluids may assume any density and viscosity contrasts. In addition, the axisymmetric profile of the tube maintains a relatively small angle of tangency to warrant that the axial velocity distribution assumes, approximately, a parabolic profile. The driving forces that may be encountered in this system include the capillary force, pressure force, gravitational force and an opposing viscous force. The orientation of the capillary force can be in the direction of the flow (e.g. during imbibition) or opposite to the flow (e.g. during drainage). Likewise, the gravitational force can be in the direction of the flow or opposite to it. In this work we account for all these possibilities. A differential equation is developed that defines the location of the meniscus with time. A fourth-order-accurate Runge–Kutta scheme has been developed to provide solutions for the different scenarios associated with this system. It is shown that the developed model reduces to those appropriate for straight tubes, which builds confidence in the modelling approach. The effects of changing the tangent along the profile of the tube, which influences the calculation of the radius of curvature of the meniscus, is also considered. Unlike the cases of straight capillary tubes, in tubes with arbitrary symmetric profiles, the friction force depends on the variations of the tube profile. Examples of converging/diverging capillary tubes that follow straight and power law profiles are investigated. In addition, the case of sinusoidal profiles has also been considered.

Key words: capillary flows, contact lines

† Email address for correspondence: amgad.salama@uregina.ca

1. Introduction

Two main types of quantitative analysis methods are at our disposal when studying a physical phenomenon. These are, namely, microscopic and macroscopic methods of analysis, which depend on the scale of the phenomenon under investigation (i.e. length and/or time scales). While microscale descriptions focus on small size domains, macroscale analysis is usually adapted to larger size domains. Since microscale analyses look for the details, they handle a larger number of degrees of freedom and generate a larger volume of data. Macroscale analysis, on the other hand, integrates and homogenizes these details and generates comparatively less data. The choice between any of these two approaches is, in fact, determined by the scale of analysis. It must, however, be stated that these two methods are not entirely independent. In fact, there are situations in which one may need to focus on the behaviour of a system at some small scale in order to gain understanding of its behaviour at a larger scale. In some other situations, some parameters (properties) at the large scale may be determined by upscaling small-scale variables. A direct example of such cases may be found on studying flows of multiphase systems in porous media. At the scale of porous media (i.e. a macroscopic scale) the continuum hypothesis may be adapted and the porous medium is replaced by a fictitious one in which the internal structure of the medium is homogenized and is replaced by a continuous one (e.g. Whittaker 1999; de Boer 2006; Salama & Van Geel 2008; Das & Hassanizadeh 2010). At the pore scale (i.e. a microscopic scale), however, the story is different and one needs to account for the complex internal structure of a real porous medium (e.g. Ovaysi & Piri 2011; Raeini, Blunt & Bijeljic 2012; Golparvar *et al.* 2018; Gueto-Felgueroso *et al.* 2018). The large-scale description of the flow of multiphase systems in porous media is described using a smaller number of macroscopic parameters (e.g. relative permeability), whereas at pore scale, no such parameters exist. Instead, the details of the interface movements, the affinity characteristics of the phases against each other, along with the detailed description of the complex internal structure of even a small-scale domain, become important and need to be resolved. The problem with this approach is that the geometrical reconstruction of a real, small-scale domain is cumbersome and involves the use of computer tomography and sophisticated tools to build such a realization. There are, however, other simplified techniques that can handle these systems and significantly alleviate many of the difficulties associated with the need to reconstruct a realization of a real porous medium domain. This is done via pore network models in which the pore space is replaced by some known geometrical shapes (e.g. spheres) and the pore throats are replaced by some other shapes (e.g. cylinders) (e.g. Joekar-Niasar *et al.* 2010; Bultreys, Van Hoorebeke & Cnudde 2015; Bashtani, Irani & Kantzas 2021; Guo *et al.* 2021). The advantages of this approach are that it is far simpler than the other one and in the same time it can benefit from the ample analytical techniques related to both imbibition and drainage processes in capillaries.

Flow of a two-phase system in capillaries is linked to the dynamic behaviour of the interface that separates the two phases. Such an interface can be convex or concave according to the affinity of the two-phase system to the wall of the tube. Such a feature divides the fluids into three categories; namely, (i) wetting (i.e. the fluid spreads over the surface), (ii) non-wetting (i.e. the fluid contracts) and (iii) neutral. This introduces forces along the contact line called interfacial tension forces, which can be in the direction of the flow or opposite to it (e.g. de Gennes, Brochard-Wyart & Quere 2004; Clift, Grace & Weber 2005). In fact, in cases when such an interfacial force dominates the other forces, the system can undergo capillary-induced flows (if the invading fluid is wetting) or otherwise no flow is induced (if the fluid is non-wetting). Capillary-induced flows are sometimes

referred to as imbibition, in which the flow is caused solely by interfacial tension forces, which drag the wetting fluid along the tube (e.g. Lucas 1918; Washburn 1921; Hammecker *et al.* 1993; Bijeljic, Markicevic & Navaz 2011). On the other hand, if the fluid is non-wetting, it cannot move along the tube unless external boosting is applied (e.g. via an applied pressure). It is interesting to compare the different applied forces that are involved in the flow of a two-phase system in capillaries. Such comparison is facilitated via the dimensionless numbers $r\Delta p/\gamma$, $\mu v/\gamma$ and $\rho g r^2/\gamma$, where r is some length scale (e.g. the radius of the tube), Δp is a global pressure difference, γ is the interfacial tension, μ is the viscosity, v is some reference velocity, g is the gravity and ρ is the density. The first number describes the influence of the driving pressure force to the capillary force, the second is the capillary number, which measures the ratio between viscous and capillary forces and the last one is the Bond number, which measures the ratio between gravitational and capillary forces. These four forces (namely, pressure, capillary, friction and gravity) are important in typical two-phase flows in capillaries. Previous studies on flows in capillary tubes have considered combinations of these forces to different extents. Most of the studied scenarios have focused on imbibition scenarios in which a wetting liquid displaces a non-wetting gaseous fluid (e.g. air) because of its ubiquitous applications. In imbibition scenarios, the three forces that play key roles are the capillary, friction and gravity forces. Imbibition has been studied extensively in the context of estimating the rate at which the meniscus moves under different conditions (e.g. Lucas 1918; Washburn 1921; Hammecker *et al.* 1993; Bijeljic *et al.* 2011). An analytical expression has been developed that links the location of the meniscus and the time ($\ell \propto \sqrt{t}$) neglecting fluid inertia (Lucas 1918; Washburn 1921). Other studies have included fluid inertia and reached the conclusion that inertial effects only appear at the very early time of the imbibition process (e.g. Young 2004; Das, Waghmare & Mitra 2012; Taroni & Vella 2012; Elizalde *et al.* 2014; Reyssat 2014; Gorce, Hewitt & Vella 2016; Salama 2021*a*). In imbibition processes, the fact that the invading fluid moves against a gaseous phase with negligible viscosity and density, may apply to some particular cases involving, for example, infiltration of rain water into soil. The more general cases in which the two fluids possess considerable viscosity and density contrasts have been recently considered under both imbibition and drainage scenarios (e.g. Fries & Dreyer 2008; Das & Mitra 2013; Ramakrishnan *et al.* 2019; Salama 2021*b*). Such cases find several applications in oil production, pharmaceutical, food industries and others. Furthermore, different scenarios with respect to the orientation of the capillary tube can show applications in which gravity can assist or oppose the flow. The effect of inertia under this generalized framework has also been considered and it was concluded that the inertial effect may only appear at the very early time of the drainage or imbibition processes. Furthermore, the case involving the movement of a wetting/non-wetting ganglion of one fluid by another immiscible one in capillaries has also been considered under different viscosity and density contrasts. With all these scenarios, there are still cases of practical importance that need to be incorporated within the same generalized framework. These are related to the case in which the cross-sectional area of the capillary tube constantly changes along the length of the tube. This case is more relevant to porous medium applications in which the seeping fluids experience tortious paths. Although there have been other studies on this topic (e.g. Xiao, Yang & Pitchumani 2006, Dereyssat *et al.* 2008; Liou, Peng & Parker 2009; Hultmark, Aristoff & Stone 2011; Kornev & Neimark 2011; Maggi & Alonso-Marroquin 2012; Wang *et al.* 2012; Budaraju *et al.* 2016; Walls, Deqidt & Bird 2016; Ashraf, Visavale & Phirani 2018, Ashraf & Phirani 2019*a*,*b*), they adhere to the special case of imbibition in which the displaced fluid is of negligible viscosity and density compared with the invading one or to the case in which the capillary tube

is asymmetric. Under these conditions, it may be possible to ignore the friction loss in the subdomain domain filled with the gas phase (e.g. Salama *et al.* 2021). While this may find applications in some scenarios (e.g. flows in the vadose zone), there are ample other applications in which the viscosity and density of the two immiscible fluids cannot be ignored (e.g. in displacing oil by water). In this work, we provide a generalization to our previously developed model that predicts the location and the speed of the meniscus with time. The model considers the case of flow of a two-phase system in capillaries with arbitrary axisymmetric cross-sections. These cases are important in the context of pore network models in which pore bodies are connected via pore throats that are idealized, in most cases, as constant cross-section three-dimensional objects (e.g. cylinders, prisms). In reality, however, pore throats are more complex in structures than such simplified cases. Cases of tapered, power law and sinusoidal pore throats have been investigated. The model accounts for immiscible fluids over a wide range of viscosity and density contrasts under both imbibition and drainage scenarios. Forces due to pressure, interfacial tension, friction and gravity are considered. The model, however, does not account for the effects of electrostatic forces that may arise upon the accumulation of charges (e.g. in the realm of diffuse double layers, Das, Guha & Mitra 2013; Das *et al.* 2014). Likewise, the effects of flow slippage at channel walls that may be relevant to nano-size tubes are not considered. In other words, the developed model may be relevant to microscale capillaries and larger.

2. Statement of the problem

In this work we are primarily concerned with the displacement of one fluid by another immiscible one in capillaries of arbitrary axisymmetric cross-sections. Two cases are investigated; namely, (i) the invading fluid is wetting, and (ii) the invading fluid is non-wetting. In the first case the interface is convex with respect to the invading fluid and is concave for the second one. Because of the continuous change of the radius of the tube along its length, the curvature of the interface also changes. The interfacial tension force, likewise, changes along the tube length. The pressure at the two reservoirs between which the tube terminals are connected are p_U at the top reservoir and p_D at the bottom reservoir. Figure 1 shows a schematic of the considered set-up with the location of the interface at a distance $h(t)$ from the bottom reservoir and where the length of the tube is H. We are particularly interested in determining the location and velocity of the interface with time. Since the geometric set-up represents a symmetric system, a one-dimensional model along the axis of symmetry employs area average quantities (e.g. the mean velocity). The interfacial tension force along the axis of symmetry not only depends on the contact angle and the radius of the tube, but also on the angle of the tangent to the wall, which changes along the wall of the tube. The radius of the tube along the length is a function of the axial location, or $r_p = r_p(z)$. In previous studies (e.g. Budaraju *et al.* 2016), under quasi-static conditions, the radius of curvature $R = R(\vartheta, z)$ has been assumed to only depend on the contact angle and the radius of the tube, which may not be quite accurate except under very restrictive scenarios ($|\mathrm{d}r_p/\mathrm{d}z| \ll 1$).

In this work, we slightly relax this restriction and consider the general case in which the radius of curvature of the interface depends, in addition, on the slope of the profile of the tube, that is $R = R(\vartheta, r_p, \mathrm{d}r_p/\mathrm{d}z)$. Another restriction with respect to the profile of the capillary tube that is relevant to this study should also be mentioned. It is stipulated that the axial velocity distribution does not significantly deviate from the parabolic profile usually encountered in laminar flows in straight tubes. In order to highlight the variations

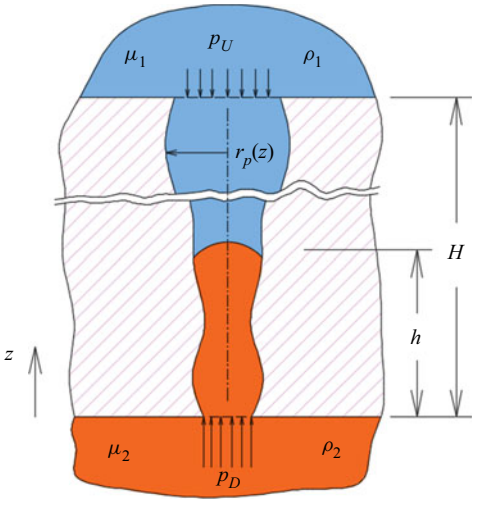

Figure 1. A non-wetting fluid (orange in colour) displaces a wetting one (blue in colour). In this case the pressure of the bottom reservoir must exceed the critical entry pressure for the interface to advance. The radius of the tube changes along its axis i.e. $r_p = r_p(z)$ in a manner that generates a converging, diverging or a combination of them along the tube.

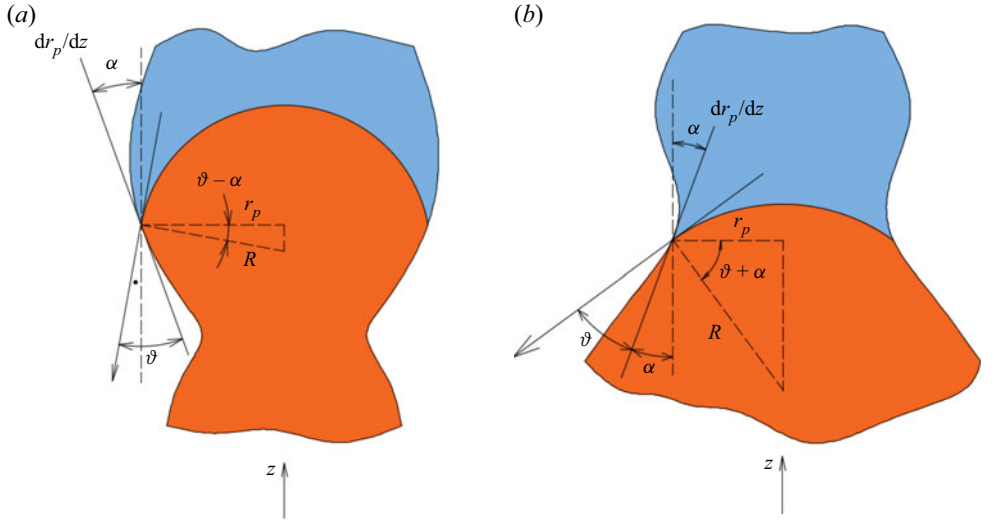

Figure 2. The radius of curvature of the interface depends not only on the contact angle and the radius of the tube but also on the slope of the profile of the tube. Two cases are to be distinguished with respect to whether the interface is at a converging or diverging portion of the tube and also with respect to whether it is an imbibition or drainage scenario. (*a*) The interface is at a diverging section. (*b*) The interface is at a converging section.

of the radius of curvature of the interface with the slope of the tube profile and its radius, consider the scenarios shown in figure 2(*a*,*b*).

The interface in this figure represents a non-wetting fluid (orange in colour) displacing a wetting one (blue in colour). At the moment when the interface is located in the diverging portion of the tube (figure 2*a*) the radius of curvature is $R = r_p/\cos(\vartheta - \alpha)$ and if the interface is at the converging portion (figure 2*b*), $R = r_p/\cos(\vartheta + \alpha)$, where

$\alpha = \tan^{-1}(\mathrm{d}r_p/\mathrm{d}z)$. As shown in figure 2, the contact angle ϑ is defined with reference to the invading liquid and the tangent of the profile of the tube. Furthermore, and for the sake of simplicity of the analysis, the dynamic nature of the meniscus is neglected and it is assumed that the contact angle ϑ remains unchanged throughout the invasion process, which may only be valid under quasi-static conditions.

3. Quasi-one-dimensional modelling approach

The control volume over which the force balance is studied spans the whole length of the capillary tube, as depicted in figure 14. It defines a capillary tube of arbitrary cross-section and a length of H connected from the top and the bottom to two reservoirs.

To simplify the analysis, we consider the upstream and downstream pressures defined right at the entrance and at the exit of the tube. In other words, the predefined pressures at the inlet and the exit of the tube account for the local losses. Although these pressures may change slightly as the pressure field evolves it is expected, over the period of simulation, that predefined volume average pressures may not vary significantly. Compared with the pressure loss along the capillary tube length, the local pressure drop at the entrance is expected to comprise only a small fraction (Budaraju *et al.* 2016). Furthermore, previous computational fluid dynamics (CFD) investigation shows a slight variation of the axial pressure profiles along the centreline in the reservoir (Salama *et al.* 2022). More discussion on local entrance losses in such set-ups can be found in several previous works, a good list of which may be found in the work of Waghmare & Mittra (2010). It is to also be mentioned that the model considers quasi-static analysis in which the contact angle is assumed fixed. The effect of the dynamic behaviour of the contact angle can be captured in a CFD study.

The conservation of linear momentum equation in integral form over a control volume may be written in a vector form as

$$\frac{\partial}{\partial t}\int_V \rho \boldsymbol{u}\,\mathrm{d}V + \int_A (\rho \boldsymbol{u}\cdot\boldsymbol{n})\boldsymbol{u}\,\mathrm{d}A = -\int_A p\boldsymbol{n}\,\mathrm{d}A + \int_A \boldsymbol{\tau}\boldsymbol{n}\,\mathrm{d}A + \int_V \rho \boldsymbol{g}\,\mathrm{d}V + \int_{CL} \gamma \boldsymbol{t}\,\mathrm{d}\ell, \tag{3.1}$$

where γ is the interfacial tension, $\boldsymbol{n}$ is the normal to the boundary unit vector, $\boldsymbol{t}$ is the unit vector normal to the contact line (CL) in the plane tangent to the interface, $\boldsymbol{u}$ is the velocity vector of the fluid crossing the boundary, $\boldsymbol{\tau}$ is the viscous stress tensor and p is the pressure. In the above equation, it is assumed that the interface intersects the boundary of the control volume. The left-hand side of the above equation represents inertia of the fluid. As mentioned earlier, the inertial effects are usually limited to the very short time period at the start of the invasion process, (e.g. Salama 2021*a*). It has been estimated elsewhere (e.g. Budaraju *et al.* 2016; Gorce *et al.* 2016) that, for the case in which the two fluids are of comparable density and viscosity, inertial effects may be important for $t \ll \rho r^2/\mu$, which is indeed small compared with the time of typical imbibition process. Therefore, it may be possible to ignore the left-hand side of (3.1). For the sake of generality, however, we drive the governing equation including the left-hand side terms. Figure 3 shows a typical capillary tube of arbitrary cross-section along with the two-phase system under both drainage (figure 3*a*) and imbibition (figure 3*b*) scenarios. If one applies the conservation of momentum law over the particular control volume shown in figure 3, the

right-hand side of (3.1) in the axial direction simplifies to

$$\sum F = [p_D A(0) - p_U A(H)] - \int_{A_1} \tau_1 \,\mathrm{d}A - \int_{A_2} \tau_2 \,\mathrm{d}A \pm \int_{V_1} \rho_1 g \,\mathrm{d}V \pm \int_{V_2} \rho_2 g \,\mathrm{d}V \pm \pi D\gamma \cos[\vartheta + \alpha(h)], \tag{3.2}$$

where p_D and p_U are the external pressure at the inlet and exit of the tube, $A(0)$ and $A(H)$ are the cross-sectional areas at the inlet and the exit, respectively, τ_1 and τ_2 are the shear stresses at the wall of the two portions of the control volume filled with both fluids, A_1 and A_2 are the surface areas of the control volume associated with the two fluid regions, V_1 and V_2 are the volumes of the respective two fluid regions, ρ_1 and ρ_2 are the densities of the fluids in the two parts, ϑ is the contact angle and α is the angle of the tangent to the tube profile as shown in figure 2. Note that the component of the pressure force in the direction of the flow exerted by the tube wall on the two-phase system is ignored due to the small angle of tangency of the tube profile. Expansion and simplifications of (3.2), yield

$$\sum F = [p_D A(0) - p_U A(H)] - 2\pi \int_h^H \tau r_p(z) \,\mathrm{d}z - 2\pi \int_0^h \tau r_p(z) \,\mathrm{d}z \pm \pi\rho_1 g \int_h^H r_p^2(z) \,\mathrm{d}z \pm \pi\rho_2 g \int_o^h r_p^2(z) \,\mathrm{d}z \pm 2\pi r_p(h)\gamma \cos[\vartheta - \alpha(h)] = 0. \tag{3.3}$$

The shear stress at the wall may be written a $\tau(z) = -\mu \partial u(z)/\partial r|_{r=r_p(z)}$. Under laminar flow conditions, which may be valid in capillaries, the velocity distribution assumes a parabolic profile and may be represented as $u(r, z) = U_{max}[1 - r^2/r_p^2(z)]$, where U_{max} is the centreline velocity. As indicated earlier, this study considers flows that are approximately uniaxial. Because of the irregular pattern of the tube profile, a cross-flow may be induced. Therefore, this analysis is valid for profiles in which the generated cross-flow is insignificant, which may be achieved when $|\mathrm{d}r_p/\mathrm{d}z| \ll 1$. In terms of the average velocity, the above equation may be written as $u(r, z) = 2\bar{U}[1 - r^2/r_p^2(z)]$, where $\bar{U}$ is the average velocity. Figure 4 shows a schematic of the parabolic profile.

Following Salama (2021*a*,*b*), substitution of the shear stress formula into (3.3) and using the volumetric flow rate, $Q = \bar{U}(z)A(z)$, to replace the average velocity, (3.3) reduces to

$$\sum F = \pi[p_D r_p^2(0) - p_U r_p^2(H)] - 8\mu_1 Q \int_h^H \frac{\mathrm{d}z}{r_p^2(z)} - 8\mu_2 Q \int_0^h \frac{\mathrm{d}z}{r_p^2(z)} \pm \pi\rho_1 g \int_h^H r_p^2(z) \,\mathrm{d}z \pm \pi\rho_2 g \int_o^h r_p^2(z) \,\mathrm{d}z \pm 2\pi r_p(h)\gamma \cos[\vartheta - \alpha(h)]. \tag{3.4}$$

The volumetric flow rate Q in terms of the time derivative of the location of meniscus can be written as $Q = [\pi r_p^2(h)]\mathrm{d}h/\mathrm{d}t$. Substitution into (3.8), simplifications and collecting terms, one obtains

$$\sum F = \pi[p_D r_p^2(0) - p_U r_p^2(H)] - 8\pi\mu_1 r_p^2(h) \left[\int_h^H \frac{\mathrm{d}z}{r_p^2(z)} + \frac{\mu_2}{\mu_1} \int_0^h \frac{\mathrm{d}z}{r_p^2(z)}\right] \frac{\mathrm{d}h}{\mathrm{d}t} \pm \pi\rho_1 g \left[\int_h^H r_p^2(z) \,\mathrm{d}z + \frac{\rho_2}{\rho_1} \int_o^h r_p^2(z) \,\mathrm{d}z\right] \pm 2\pi r_p(h)\gamma \cos[\vartheta - \alpha(h)]. \tag{3.5}$$

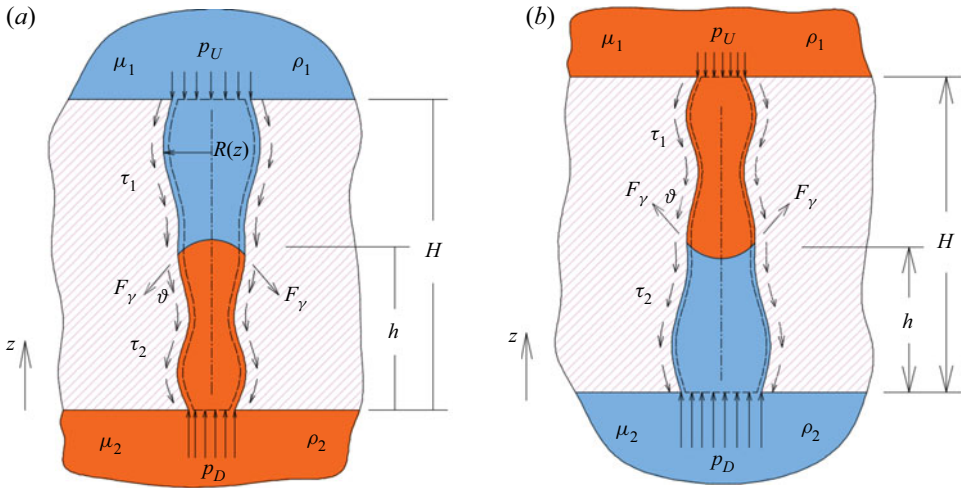

Figure 3. Schematic of the control volume (dashed line) over which force balance is performed. (*a*) Drainage and (*b*) imbibition.

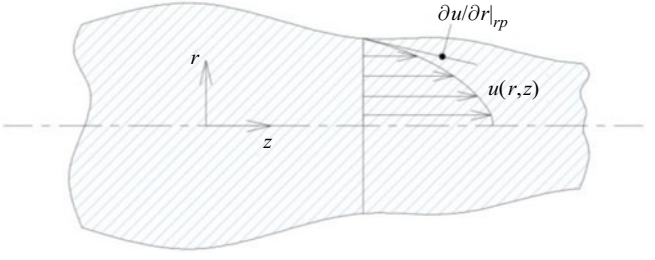

Figure 4. The axial velocity along the radius of the tube may be considered to assume a parabolic profile under laminar flow conditions.

For simplification of notation, we define the following terms $a(h) = \int_h^H \mathrm{d}z/r_p^2(z)$, $b(h) = \int_0^h \mathrm{d}z/r_p^2(z)$, $c(h) = \int_h^H r_p^2(z)\,\mathrm{d}z$ and $e(h) = \int_o^h r_p^2(z)\,\mathrm{d}z$.

Substitution into (3.5), one obtains

$$\sum F = [p_D A(0) - p_U A(H)] - \left[8\mu_1 \pi r_p^2(h)\left(a + b\frac{\mu_2}{\mu_1}\right)\right]\frac{\mathrm{d}h}{\mathrm{d}t}$$
$$\pm \pi\rho_1 g\left[c + \frac{\rho_2}{\rho_1}e\right] \pm 2\pi r_p(h)\gamma\cos(\vartheta - \alpha). \tag{3.6}$$

One may define the following two terms, $\lambda = \mu_2/\mu_1$, and $\xi = \rho_2/\rho_1$. On substitution into (3.6), one obtains

$$\sum F = [p_D r_p^2(0) - p_U r_p^2(H)] - [8\mu_1 r_p^2(h)(a + b\lambda)]\frac{\mathrm{d}h}{\mathrm{d}t}$$
$$\pm \rho_1 g(c + e\xi) \pm 2r_p(h)\gamma\cos(\theta - \alpha). \tag{3.7}$$

On the other hand, the left-hand side of (3.1) may be written as

$$\text{LHS} = \frac{\partial}{\partial t}\rho(h)A(h)\frac{\partial h}{\partial t} + \rho_1\left(\frac{1}{A(0)} - \frac{\rho_2/\rho_1}{A(H)}\right)A^2(h)\left(\frac{\partial h}{\partial t}\right)^2, \tag{3.8}$$

where $\rho(h) = \rho_2 h + \rho_1(H-h)$, $A(0)$, $A(H)$ and $A(h)$ are the cross-section areas at the inlet, exit and at the location of the meniscus, respectively. The general form of the equation may, therefore, be written as

$$\begin{aligned}\frac{\mathrm{d}}{\mathrm{d}t}\left[\rho(h)A(h)\frac{\mathrm{d}h}{\mathrm{d}t}\right] + \rho_1\left(\frac{1}{A_U} - \frac{\rho_2/\rho_1}{A_D}\right)A^2(h)\left(\frac{\mathrm{d}h}{\mathrm{d}t}\right)^2 \\ = [p_D r_p^2(0) - p_U r_p^2(H)] - [8\mu_1 r_p^2(h)(a+b\lambda)]\frac{\mathrm{d}h}{\mathrm{d}t} \pm \rho_1 g(c+e\xi) \\ \pm 2r_p(h)\gamma\cos(\theta-\alpha).\end{aligned} \tag{3.9}$$

Equation (3.9) is a second-order, nonlinear ordinary differential equation. For the sake of simplicity, if it is possible to ignore the left-hand side terms based on the discussion presented earlier, the above equation reduces to

$$\begin{aligned}[p_D r_p^2(0) - p_U r_p^2(H)] - [8\mu_1 r_p^2(h)(a+b\lambda)]\frac{\mathrm{d}h}{\mathrm{d}t} \\ \pm \rho_1 g(c+e\xi) \pm 2r_p(h)\gamma\cos(\theta-\alpha) = 0.\end{aligned} \tag{3.10}$$

Which for spontaneous imbibition, simplifies to

$$2r_p(h)\gamma\cos(\theta-\alpha) = \rho_1 g[c(h)+e(h)\xi] + \{8\mu_1 r_p^2(h)[a(h)+b(h)\lambda]\}\frac{\mathrm{d}h}{\mathrm{d}t}. \tag{3.11}$$

Similarly, for upward drainage scenarios, (3.10) may be reformulated as

$$\begin{aligned}p_D r_p^2(0) = p_U r_p^2(H) + \rho_1 g[c(h)+e(h)\xi] + 2r_p(h)\gamma\cos[\vartheta+\alpha(h)] \\ + \{8\mu_1 r_p^2(h)[a(h)+b(h)\lambda]\}\frac{\mathrm{d}h}{\mathrm{d}t}.\end{aligned} \tag{3.12}$$

Equation (5.2) represents a model that can handle the invasion process in capillaries of arbitrary shape under the assumption that inertia may be neglected. As seen, (3.10) is a first-order, nonlinear, differential equation for which it may be difficult to find an analytical solution. Furthermore, the integral coefficients a, b, c and e may not always reduce to a closed form. Therefore, a fourth-order Runge–Kutta scheme has been adapted in this study to solve this system.

4. Verification and validation

The case of imbibition and drainage in straight capillaries under the same framework has been considered in Salama (2021*a*,*b*). In this section, we show that this developed generalized model reduces to those previously developed models in straight capillary tubes. In this case $r_p(z) = \text{const.}$, and $\alpha = 0$. The integral coefficients are as follows:

$a = (H - h)/r_p^2$, $b = h/r_p^2$, $c = r_p^2(H - h)$ and $e = r_p^2 h$. Substitution yields

$$[p_D r_p^2(0) - p_U r_p^2(H)] - 8\mu_1[H - h + h\lambda]\frac{\mathrm{d}h}{\mathrm{d}t} \pm \rho_1 g r_p^2[H - h + h\xi] \pm 2r_p\gamma\cos(\vartheta) = 0. \tag{4.1}$$

Collecting terms

$$(p_D - p_U) - \frac{8\mu_1}{r_p^2}[H + h(\lambda - 1)]\frac{\mathrm{d}h}{\mathrm{d}t} \pm \rho_1 g[H + h(\xi - 1)] \pm \frac{2\gamma\cos\vartheta}{r_p} = 0. \tag{4.2}$$

Factoring

$$\Delta p \pm \frac{2\gamma\cos\vartheta}{r_p} \pm \rho_1 g H\left[1 + \frac{h}{H}(\xi - 1)\right] - \frac{8\mu_1 H}{r_p^2}\left[1 + \frac{h}{H}(\lambda - 1)\right]\frac{\mathrm{d}h}{\mathrm{d}t} = 0. \tag{4.3}$$

Rearrangement

$$\left(\Delta p \pm \frac{2\gamma\cos\vartheta}{r_p} \pm \rho_1 g H\right) \pm \rho_1 g h(\xi - 1) - \frac{8\mu_1 H}{r_p^2}\left[1 + \frac{h}{H}(\lambda - 1)\right]\frac{\mathrm{d}h}{\mathrm{d}t} = 0. \tag{4.4}$$

This last equation is identical to that developed in Salama (2021*b*), which applies to any combination of two immiscible fluids in capillaries over a large spectrum of density and viscosity contrasts. Furthermore, for spontaneous imbibition in horizontal capillaries between a wetting liquid and air, we have, $\rho_1 \approx 0$, $\mu_1 \approx 0$, $\Delta p = 0$ and $g = 0$, and (4.1) reduces to

$$h\frac{\mathrm{d}h}{\mathrm{d}t} = \frac{\gamma r_p\cos\vartheta}{4\mu_2}. \tag{4.5}$$

The solution of the above equation is $h = \sqrt{(\gamma r_p t\cos\vartheta)/2\mu}$, which is the celebrated Washburn–Lucas equation. Note that the subscript of μ_2 has been dropped for simplicity of notation. Another verification exercise is considered for a case in which the profile of the tube varies. We consider a converging diverging tube as depicted in figure 5(*a*). The tube profile shows three straight sections connected with two necks representing a converging and a diverging section, (Erickson, Li & Park 2002). Figure 5(*b*) shows a comparison between the current model and that of Erickson *et al.* (2002), who considered the special case of spontaneous imbibition in the system shown in figure 5(*a*), and as seen, a good match is obtained. The developed model, however, can handle the general case of a two-phase system with arbitrary viscosity and density contrasts with/without gravity.

Now, having established the generalized model, it is time to consider some special cases. Three special geometries are considered in the next sections; namely, (i) straight converging/diverging capillaries, (ii) power law capillary profiles and (iii) a sinusoidal profile. In all the considered scenarios, $\mathrm{d}r_p/\mathrm{d}z \ll 1$. Conditions and assumptions of each of the considered scenarios are summarized in table 1 below.

5. Quasi-one-dimensional model for capillary flow in a converging/diverging straight tube

Consider the case in which the capillary tube is of a cross-section that changes linearly along the tube length. Two scenarios are possible; namely a converging profile in which the diameter decreases along the length, and a diverging profile when the diameter increases

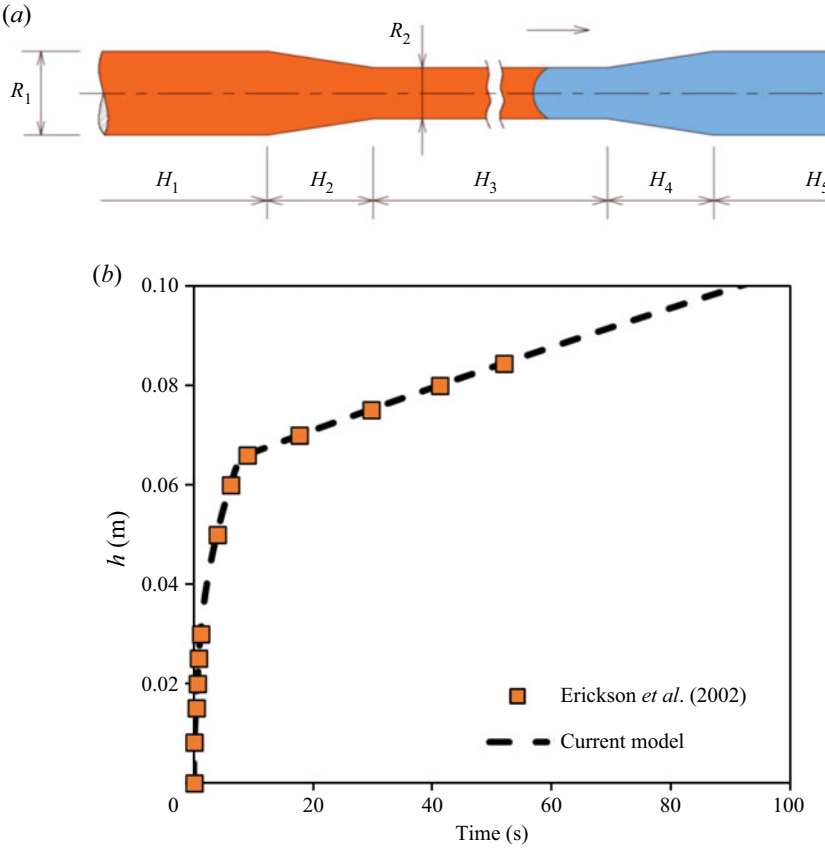

Figure 5. Schematic of the tube profile (*a*) as given in Erickson *et al.* (2002) that is been used for the comparison and (*b*) comparison of the location of the meniscus with time. The dimensions are $H_1 = 20$ mm, $H_2 = 2.8647$ mm, $H_3 = 40$ mm, $H_4 = 2.8647$ mm, $H_5 = 35$ mm, $R_{max} = 50$ μm and $R_{min} = 25$ μm, and the properties of the imbibing fluid are $\rho = 1000$ kg m^{-3}, $\gamma = 0.03$ N m^{-1} and $\vartheta = 30^{\circ}$.

A converging linear profile	Imbibition scenario, fluid inertia is ignored, no gravity, no electrostatic effects are considered
A diverging linear profile	Imbibition scenario, local and convective inertia are ignored, no gravity, no electrostatic effects are considered
A converging quadratic profile	Imbibition scenario1, local and convective inertia are ignored, no gravity, no electrostatic effects are considered Imbibition scenario2, local and convective inertia are ignored, with gravity, no electrostatic effects are considered
A diverging quadratic profile	Imbibition scenario1, local and convective inertia are ignored, no gravity, no electrostatic effects Imbibition scenario2, local and convective inertia are ignored, with gravity, no electrostatic effects
A sinusoidal profile	Imbibition scenario1, local and convective inertia are ignored, no gravity, no electrostatic effects Imbibition scenario2, local and convective inertia are ignored, with gravity, no electrostatic effects

Table 1. Scenarios considered in this work.

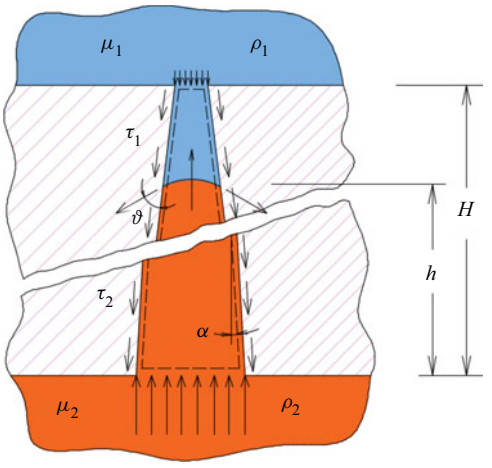

Figure 6. Tapered straight capillary tube in the drainage scenario. The orange-coloured region is filled with the non-wetting fluid while the blue-coloured region is the wetting fluid.

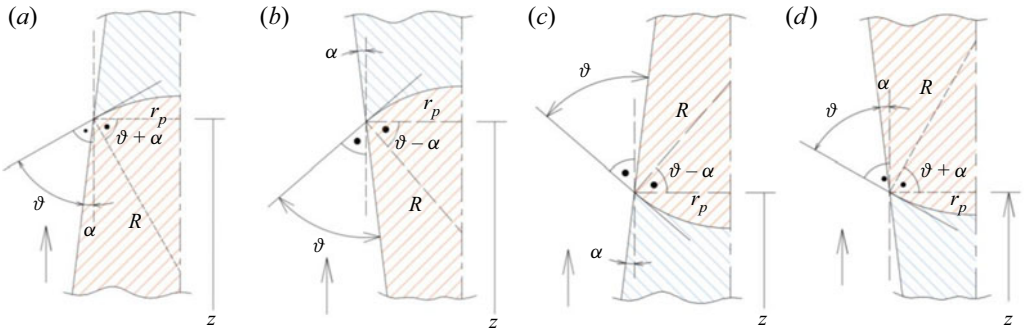

Figure 7. Interface in tapered straight tube under imbibition and drainage scenarios. The angle between the direction of the interfacial tension force and the axial direction (z-direction) is given by $\vartheta \pm \alpha$, where α is the angle between the tangent to the tube profile and the z-direction. (*a*) Drainage (converging profile), (*b*) drainage (diverging profile), (*c*) imbibition (converging profile) and (*d*) imbibition (diverging profile).

along the length. A generalized linear equation may be written as

$$r_p(z) = r_p(0) + \frac{r_p(H) - r_p(0)}{H} z. \tag{5.1}$$

Which in standard form may be written as $r_p = mz + \mathscr{b}$, where the slope $m = [r_p(H) - r_p(0)]/H$ can be positive or negative and intercepts $\mathscr{b} = r_p(0)$, $\mathscr{b} > 0$. Figure 6 shows a schematic of one such scenario (the converging profile) in a drainage process. Figure 7, on the other hand, shows the interface as it intersects with the tube wall for both imbibition and drainage scenarios. It is worth mentioning that the angle which the interfacial tension force makes with the axial direction in the drainage scenario is opposite to that in the imbibition scenario, as depicted in figure 7. That is, for example in a converging capillary straight tube, under the drainage scenario, the angle is $(\vartheta + \alpha)$, and for imbibition scenario it is $(\vartheta - \alpha)$. The solution of (3.10) requires the determination of the four parameters a, b, c and e. Luckily, for this scenario, analytical expressions for these parameters may be obtained by evaluating the integrations, as listed in table 1.

It is interesting to highlight some key features of this system by comparing the speed of the meniscus at the beginning (i.e. when it is at the entrance) and at the exit of the tube. For simplicity, we consider a spontaneous imbibition scenario in horizontal capillaries. In this case (4.4) reduces to

$$\frac{\mathrm{d}h}{\mathrm{d}t} = \frac{2\gamma\cos(\theta+\alpha)/r_p(h)}{\{8\mu_1[a(h)+b(h)\lambda]\}}. \tag{5.2}$$

Table 1 Analytical expressions for the parameters a, b, c and e for the cases of imbibition and drainage in converging/diverging straight capillaries.

$a(h)$	$\dfrac{1}{m(mh+\mathscr{b})} - \dfrac{1}{m(mH+\mathscr{b})}$	(5.3)
$b(h)$	$\dfrac{1}{m\mathscr{b}} - \dfrac{1}{m(mh+\mathscr{b})}$	(5.4)
$c(h)$	$\dfrac{(mH+\mathscr{b})^3}{3m} - \dfrac{(mh+\mathscr{b})^3}{3m}$	(5.5)
$e(h)$	$\dfrac{(mh+\mathscr{b})^3}{3m} - \dfrac{\mathscr{b}^3}{3m}$	(5.6)
$\alpha(h)$	$\tan^{-1}(m)$	(5.7)

Substitution of the parameters $a(h)$ and $b(h)$ as given in (5.3) and (5.4), yields

$$\frac{dh}{dt} = \frac{\gamma\cos(\theta+\alpha)/r_p(h)}{\left\{4\mu_1\left[\dfrac{1}{m(mh+\mathscr{b})} - \dfrac{1}{m(mH+\mathscr{b})} + \left(\dfrac{1}{m\mathscr{b}} - \dfrac{1}{m(mh+\mathscr{b})}\right)\lambda\right]\right\}} \tag{5.8}$$

With simplifications and rearrangements, one finds

$$\frac{dh}{dt} = \frac{\gamma\cos(\theta+\alpha)/r_p(h)}{\left\{4\mu_1\left[\dfrac{1}{m(mh+\mathscr{b})} - \dfrac{1}{m(mH+\mathscr{b})} + \left(\dfrac{1}{m\mathscr{b}} - \dfrac{1}{m(mh+\mathscr{b})}\right)\lambda\right]\right\}} \tag{5.9}$$

Therefore, at the beginning of the imbibition process (i.e. $h=0$), (5.9) simplifies to

$$u(0) = \left.\frac{\mathrm{d}h}{\mathrm{d}t}\right|_{h=0} = \frac{\gamma\cos(\theta+\alpha)r_p(H)}{4\mu_1 H}. \tag{5.10}$$

Furthermore, when $h=H$ one obtains

$$u(H) = \left.\frac{\mathrm{d}h}{\mathrm{d}t}\right|_{h=H} = \frac{\gamma\cos(\theta+\alpha)r_p(0)}{4\mu_1\lambda H}. \tag{5.11}$$

Now, the ratio between the velocities of the meniscus at the exit and at the inlet is

$$\frac{u(H)}{u(0)} = \frac{r_p(0)/r_p(H)}{\lambda}. \tag{5.12}$$

For the special case in which $r_p(0)/r_p(H)=\lambda$, the velocity ratio is one, which implies that the meniscus moves at a constant speed. Furthermore, if $r_p(0)/r_p(H)>\lambda$, the speed of

the meniscus increases and decreases otherwise. It is interesting to notice that, if $r_p(0) = r_p(H)$, which corresponds to the case of a straight uniform tube, the velocity ratio is $1/\lambda$. For the case of a diverging tube in which $r_p(0)/r_p(H) < 1$, $u(H)$ is always smaller than $u(0)$. One can also investigate the ratio of the velocities of the meniscus at the exit of the tube for different converging or diverging scenarios for the same fluids. For two profiles of different angles α but the same$r_p(0)$, the ratio of the velocities is $u_1(H)/u_2(H) = \cos(\theta + \alpha_1)/\cos(\theta + \alpha_2)$. For longer tubes, α is usually small, which leads to$u_1(H) \approx u_2(H)$. This is interesting and is a manifestation of the fact that when the meniscus reaches the exit, the tube becomes filled with only the invading fluid. In this case the friction force will only depend on the size of the tube, and both the friction and the capillary forces are oppositely correlated with the size of the pore. Therefore, for the smaller size pore opening at the exit, the capillary force increases and likewise the friction force and this seems to cancel out their effect. Likewise, for the same $r_p(0)$, the ratio between the velocities of the meniscus at the beginning of its movement is

$$\frac{u_1(0)}{u_2(0)} = \frac{\cos(\theta + \alpha_1)[r_p(H)]_1}{\cos(\theta + \alpha_2)[r_p(H)]_2}. \tag{5.13}$$

Which, again for longer tubes, simplifies to $u_1(0)/u_2(0) \approx [r_p(H)]_1/[r_p(H)]_2$. This may be read as follows: for the same fluids and $r_p(0)$, the inlet velocity is larger the larger the size of the opening at the exit. This conclusion, in fact, should come as no surprise on account of the fact that the larger size pore opening implies less overall resistance, hence the above observation. An analytical expression can be derived that depicts the dynamics of the meniscus along the tube length. A derivation can be found in Appendix A. It takes the form

$$\frac{(\lambda - \beta)}{2H\psi}h^2 + \frac{\beta}{\psi}h = t, \tag{5.14}$$

where $\beta = r_p(0)/r_p(H)$, and $\psi = \gamma r_p(0)\cos(\theta + \alpha)/4\mu_1 H$. These conclusions are manifested on applying the developed model on the two cases of imbibition in converging and diverging straight capillaries. In all the considered scenarios, the viscosity ratio between the invading fluid and the displaced one is set to 100, the surface tension to 0.072 N m^{-1} and the contact angle is 45°. Starting with the case of imbibition in converging straight pipes in which the radius of the tube at the inlet, $r_p(0)$, for all the scenarios is set to 0.0005 m. At the exit, the tube assumes radii of 5×10^{-4}, 5×10^{-5}, 2.5×10^{-5}, 1.25×10^{-5}, 5×10^{-6} and 1.25×10^{-6} m. This corresponds to radius ratios, i.e. $r_p(H)/r_p(0)$, of 1.0, 0.1, 0.05, 0.025, 0.01 and 0.0025, respectively, with the case in which the radius ratio is 1 representing a straight tube. Figure 8 shows the location of the meniscus along the tube with time for the different scenarios. It is more appropriate to scale the time by $T = 2\mu H^2/\gamma r_p(0)\cos\vartheta$, which represents the total time at which the meniscus would reach the exit of the straight tube. As has been stated earlier, the scenario in which the radius ratio equals the viscosity ratio defines the boundary between the two cases. In the first case, in which $r_p(H)/r_p(0) > 1/\lambda$, after the initial period, the velocity of the meniscus decelerates with time. This implies that the friction force dominates the capillary force in these cases. In the second case, i.e. when $r_p(H)/r_p(0) < 1/\lambda$, the opposite occurs and the meniscus accelerates, which indicates that the capillary forces dominate the viscous force. When $r_p(H)/r_p(0) = 1/\lambda$, the meniscus moves at a constant speed. These conclusions, which have been deduced from analysing the model, are confirmed as depicted in figure 8.

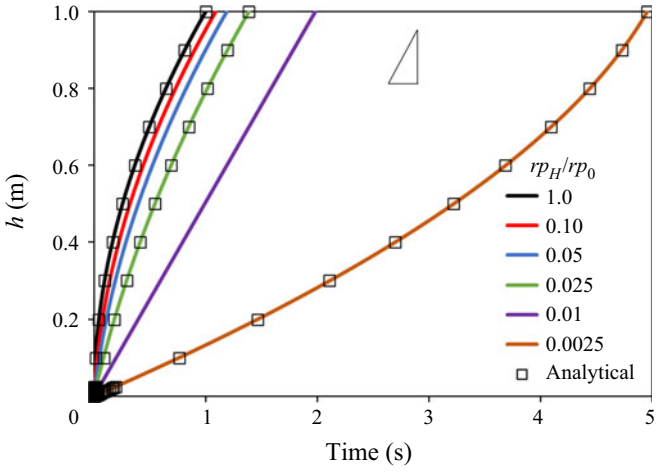

Figure 8. The normalized location of the meniscus along the tube for the different converging scenarios. When the radius ratio equals the viscosity ratio, the speed of the meniscus is constant and, in this case, the capillary force and viscous force balance each other ($h^* = h/H,\ t^* = t/T$).

Furthermore, the exit speed of the meniscus is approximately the same for the different scenarios, which is also seen in figure 8. That is, the slopes at the end of these curves (which represents the velocity) are indeed approximately the same. This is also manifested in figure 9, which shows the profiles of the speed of the meniscus with time for the different scenarios. At the exit, the speed of the meniscus, for all the scenarios, converges to almost the same speed. This has been highlighted in the earlier discussion and indicates the fact that the interplay between viscous and capillary forces is such that they both increase along the tube length. At the start of the imbibition process, the initial velocity is dictated by the initial overall resistance of the tube, which is larger the narrower the tube at the exit. In other words, when the meniscus is at the inlet of the tube, for all the scenarios, the capillary force, which is approximately identical at the start, is opposed by larger viscous resistance when the size of the pore at the exit is smaller. This leads the meniscus to acquire a larger initial speed when the size of the tube at the exit is larger and *vice versa*. This behaviour is manifested in figure 9, which shows the velocity profiles of the meniscus for the different scenarios.

When the meniscus is at the exit, on the other hand, the larger overall viscous resistance when the exit of the tube is smaller is counteracted by a larger capillary force. In other words, the capillary force at the exit of the tube is not the same for all the scenarios and this explains the noticed behaviour.

The case of a diverging straight tube is also considered in this work. The radius of the tube at the inlet for all the scenarios has been set to 0.00005 m and at the exit, it follows radius ratios, $r_p(H)/r_p(0)$, of 1, 5, 10, 25 and 50. Unlike the converging scenario, the location of the meniscus for all the scenarios of a diverging tube follows a relatively similar profile as depicted in figure 10. The fact that there is no significant difference in the profiles that depict the location of meniscus in all the scenarios is interesting and is a reflection of the interplay between viscous and capillary forces, with both decreasing along the tube length. When the meniscus is at the inlet of the tube, the capillary force for all the scenarios is approximately similar. However, the overall friction force is different for the different scenarios with it being larger the smaller the size of the tube at the exit.

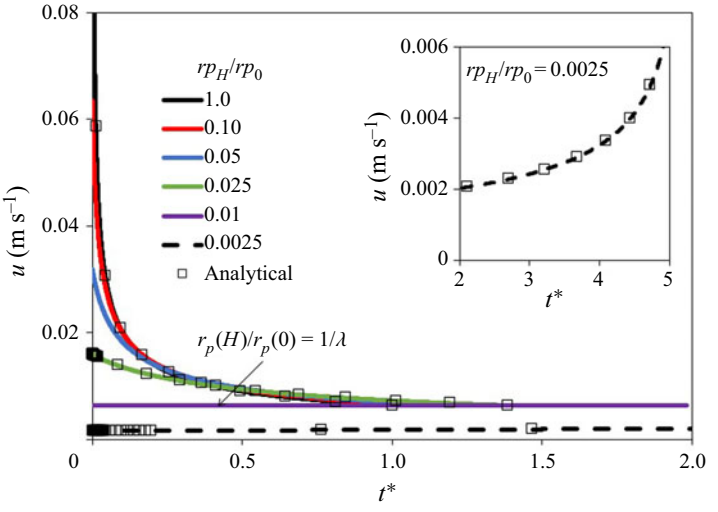

Figure 9. Velocity profiles for the case of a converging straight tube. The ratio of the radius of the tube between the exit and the inlet, i.e. $r_p(H)/r_p(0)$, changes between 1 (for straight tube) and 0.0025. The speed of the meniscus drops initially at a faster pace then at a lower rate towards the end until the meniscus reaches the exit. (Note the time is normalized by $T = 2\mu H^2/\gamma r_p(0)\cos\vartheta$.)

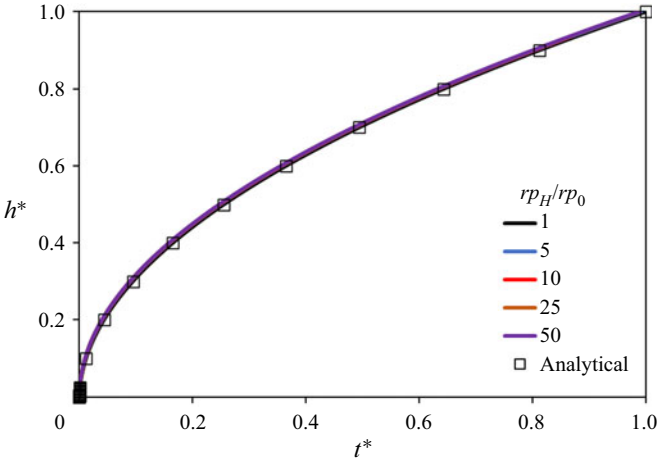

Figure 10. Profiles of the location of the meniscus with time (normalized by $T = 2\mu H^2/\gamma r_p(0)\cos\vartheta$) for the different diverging profile cases. The radius at the exit of the tube changes between 1 (for straight tube) and 50 times of that at the inlet. As seen, the profiles look similar for all the cases.

Therefore, we would expect there are variations of the speed of the menisci at the inlet, which is indeed depicted in figure 11. At the exit, the story is opposite to that of the converging tube scenario. That is, the capillary force at the exit becomes smaller compared with its value at the inlet. The lowest capillary force would occur when the meniscus reaches the exit of the tube (i.e. at the larger cross-section) and likewise the friction force. This simply leads the speed of the meniscus at the exit to be almost the same, which conforms to the discussion outlined earlier. A more detailed discussion about the effects of the different geometrical factors (i.e. the parameters a, b, $r_p(h)$) on both the friction and capillary forces is given in Appendix B. It highlights how the friction and capillary

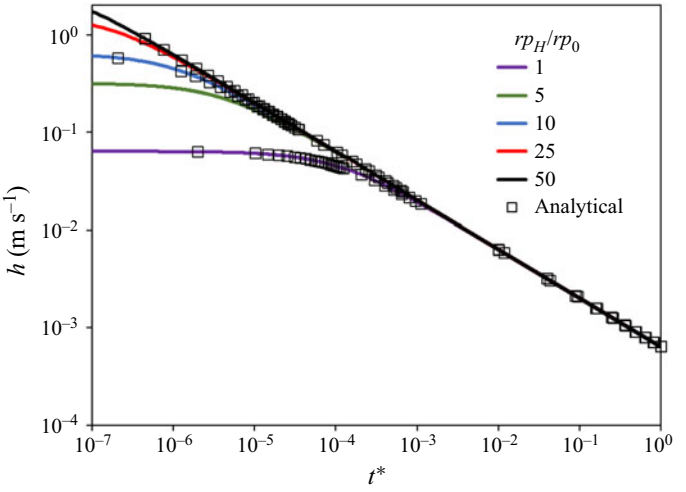

Figure 11. Velocity profiles for the diverging scenarios on a logarithmic scale. The velocities at the start are different and they converge at the end.

forces change along the tube length, and how this explains the different behaviour of the meniscus along the tube.

6. Quasi-one-dimensional model for power-law-shaped converging/diverging capillaries

This is another interesting case in which the tube assumes a nonlinear profile. Both converging and diverging profiles are considered. The interesting thing in this case is the fact that the angle of tangency along the tube length (i.e. α) changes continuously and should be incorporated as a variable rather than just a constant. Moreover, the influence of the angle of tangency is expected to show an influence on the profiles of the speed of the meniscus. In this scenario, the profile of the tube takes the general form as given below

$$r_p(z) = r_p(0)\epsilon z^n, \quad n > 1, \tag{6.1}$$

where ϵ is a parameter with its sign defines whether the profile is converging (i.e. when $\epsilon < 0$) or diverging (i.e. when $\epsilon > 0$). If $r_p(H)$ is known *a priori*, then $\epsilon = [r_p(H) - r_p(0)]/H^n$.

We define $r_p^*{=}r_p(z)/r_p(0)$, $z^* = z/H$ and $\omega = \epsilon H^n/r_p(0)$, (6.1) may, therefore, be written in a dimensionless form as

$$r_p^*{=}1 + \omega(n)z^{*n}. \tag{6.2}$$

Figure 12(*a*) shows a diverging profile for the case when $n = 2$, and $\omega = 1.0$. Similarly, figure 12(*b*) shows a converging one when $n = 2$, and $\omega = -0.5$. For the sake of illustration, we consider imbibition scenarios over quadratic profiles (i.e. the exponent n is 2). For this profile, the analytical expressions for the parameters a, b are long and complex, however, they are relatively simple for the other two parameters c, and e, which are expressed as

$$c(h) = \frac{3H^5\epsilon^2 + 10H^3 r_p(0)\epsilon + 15Hr_p^2(0)}{15} - \frac{3h^5\epsilon^2 + 10h^3 r_p(0)\epsilon + 15hr_p^2(0)}{15}, \tag{6.3}$$

$$e(h) = \frac{3h^5\epsilon^2 + 10h^3 r_p(0)\epsilon + 15hr_p^2(0)}{15}. \tag{6.4}$$

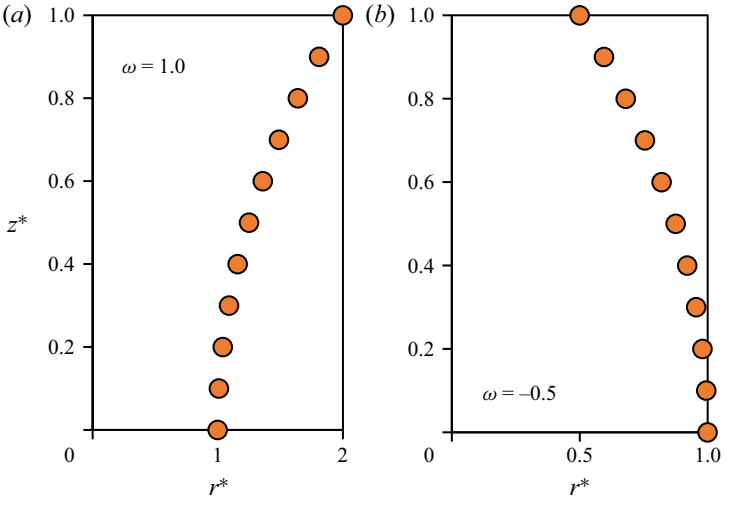

Figure 12. Two normalized quadratic profiles as an example of a power law capillary tube. (*a*) A diverging profile and (*b*) a converging profile.

Furthermore, the slope of the tube profile changes along the tube length. The slope will be negative for the converging profile and positive otherwise. It may be given as

$$\alpha(h) = \frac{\mathrm{d}r_p}{\mathrm{d}z} = 2\epsilon h. \tag{6.5}$$

We first investigate the case of a converging quadratic profile. In this case, the radius of the tube at the inlet is considered as 0.005 m and at the exit it takes a value corresponding to the radius ratios of 1.0, 0.1, 0.05, 0.01 and 0.005, respectively. Figure 13 shows the profiles of the location of the meniscus with time for the different scenarios. Apart from the straight tube profile, which shows that the profile steadily progresses with a decreasing slope, for the case of a quadratic converging profile the slope changes in a different manner, as depicted in figure 13. The slope of the profile of the location of the meniscus decreases at early times, implying a decrease in the velocity of the meniscus, it then increases again, implying an increase in the velocity of the meniscus. This can be explained in light of the relationship between capillary and friction forces. During the early time, the friction force dominates and this leads to a decrease in the velocity of the meniscus. Later on, the capillary force takes over and this results in an increase in the velocity of the meniscus. More insight into this can be found in Appendix B in the context of converging straight tubes. Furthermore, the profiles show that the meniscus takes longer to reach the end of the tube when the radius ratio is smaller, which is a manifestation of the increased friction.

This behaviour is also depicted in figure 14, which shows the profile of the speed of the meniscus for the different scenarios. It is clear that the speed of the meniscus drops at the start at a faster pace, plateaus, then increases again. This is interesting and implies, as mentioned before, that at the beginning the friction force grows quickly (faster than the capillary force), reducing thereby the speed of the meniscus. The two forces then approximately balance each other and the speed of the meniscus plateaus. Towards the end, the capillary force takes over and the speed of the meniscus increases. To highlight the initial speed of the meniscus for the different scenarios at the start of the imbibition process, figure 15 is a reproduction of figure 14 on a logarithmic scale. It shows the speeds

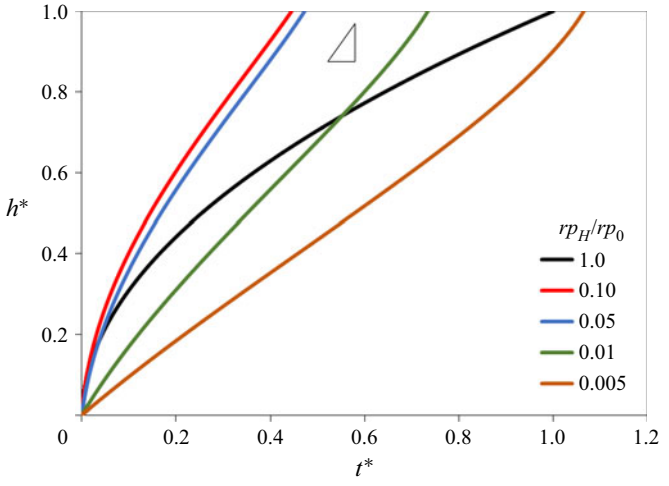

Figure 13. Profiles of the location of the meniscus along the tube for different radius ratios for quadratic converging tube profiles.

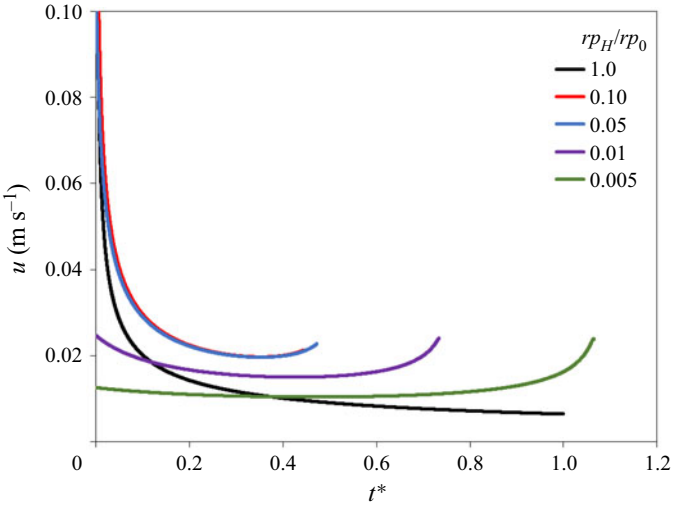

Figure 14. Velocity profile of the meniscus with time for the quadratic converging tube profile. Three time periods can be identified, namely, (i) a period at the start where the speed drops, (ii) a period in the middle where the speed plateaus and (iii) a period at the end where the speed increases.

of the meniscus at the start of the imbibition process (they are different) and likewise at the end (they are approximately the same).

For the case of a diverging quadratic profile, the radius of the tube at the entrance for all the scenarios is considered as 0.00005 m. At the exit, the radius of the diverging tube varies according to radius ratios of 1, 5, 10, 25 and 50. Figure 16 shows the profiles of the location of the meniscus along the tube and, as depicted, the time spans until the meniscus reaches the end of the tube are different (being longer when the tube radius at the exit is larger). This is unlike the case when the diverging tube follows a linear pattern, which shows relatively similar profiles as shown in figure 10. This may be explained in light of the

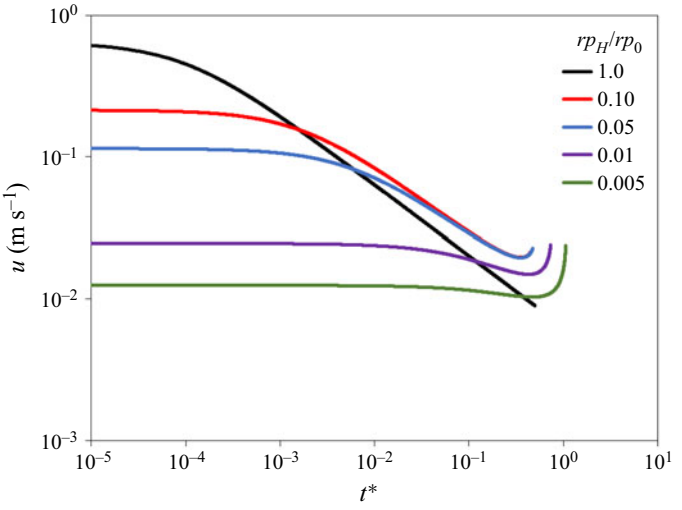

Figure 15. Velocity profile of the meniscus over a logarithmic scale for the converging, quadratic tube profile.

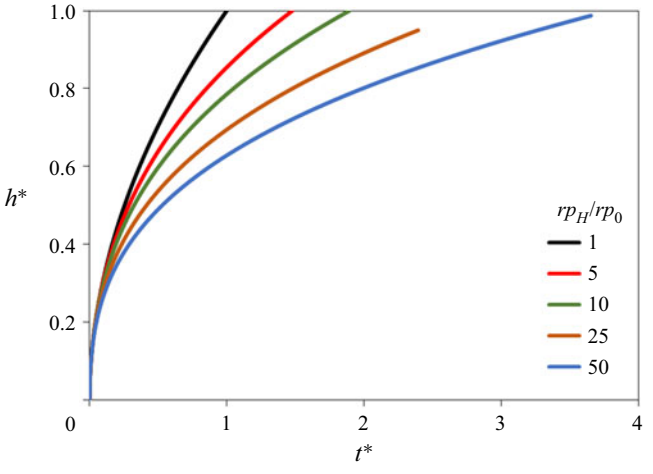

Figure 16. The profile of the location of the meniscus (normalized by the length of the tube) with time normalized by the total time the meniscus needs to reach the exit of a straight tube (i.e. $T = 2\mu H^2/\gamma r_p(0)\cos\vartheta$).

behaviour of the friction and capillary forces along the tube. It is evident that the friction force increases with the nonlinear increase in the tube diameter along its length more than the increase in capillary force. This results in the speed of the meniscus decreases as the diameter ratio increases and explains the longer time it takes for the meniscus to reach the end of the tube as the diameter ratio increases. More insight can be inferred from the discussion presented in Appendix B.

Velocity profiles, likewise, drop at a faster rate at the start and then at a slower rate, as depicted in figure 17. To capture the variations of the velocity of the meniscus at the start and at the end, figure 17 is reproduced over a logarithmic scale, which is illustrated in figure 18.

As depicted, the initial velocity is larger the larger the diameter ratio. At the end, however, it is interesting to note that, unlike the case of a diverging straight tube where

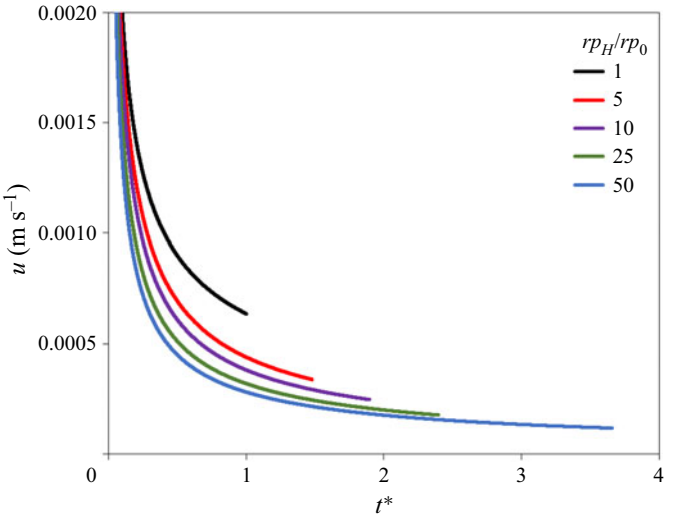

Figure 17. Velocity profile for a diverging quadratic tube profile on a linear scale.

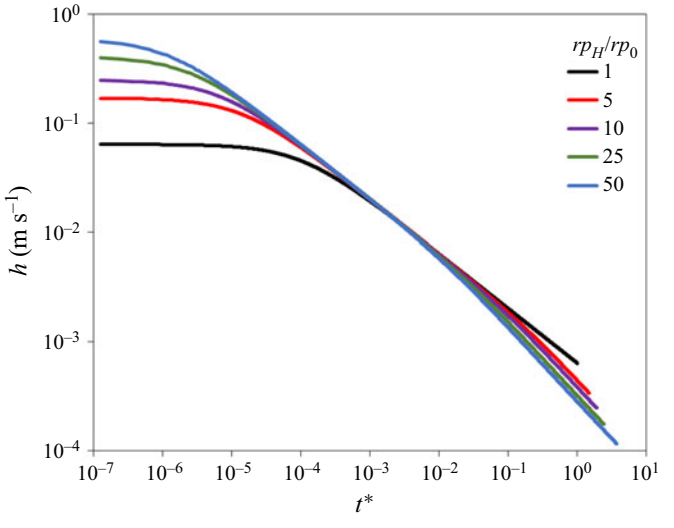

Figure 18. Velocity profile for a diverging quadratic tube profile on a logarithmic scale.

the velocity at the exit is similar for all the scenarios, this is not the case when the tube profile is nonlinear. This may be explained as previously mentioned in relation to the ratio $u_1(H)/u_2(H) = \cos(\theta + \alpha_1)/\cos(\theta + \alpha_2)$. When the tube is nonlinearly diverging, the angles α_1, and α_2 may not be ignored and this explains the noticed behaviour.

7. Quasi-one-dimensional model for sinusoidal-shaped capillaries

This is an interesting scenario because it involves both converging and diverging parts in one profile. A general sinusoidal profile takes the form

$$r_p = \frac{r_{p,max} - r_{p,min}}{2} \sin\left(2\pi \frac{z}{\varepsilon}\right) + \frac{r_{p,max} + r_{p,min}}{2}, \tag{7.1}$$

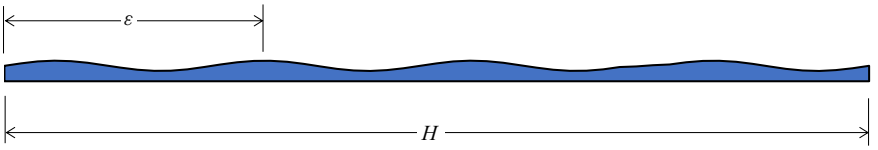

Figure 19. Schematic of a capillary tube with sinusoidal profile.

where ε is the wavelength and is chosen such that $\varepsilon/H \sim O(1)$, as depicted in figure 19. Let $A = (r_{p,max} - r_{p,min})/2$, and $B = (r_{p,max} + r_{p,min})/2$, then the above equation simplifies to

$$r_p = A\sin(Bz) + C. \tag{7.2}$$

In accordance with lubrication theory (Budaraju *et al.* 2016), it may be required that $A \ll 1$, which may also be translated as $\mathrm{d}r_p/\mathrm{d}z \ll 1$. This implies that the transverse length scale of the flow is small compared with the length scale in the flow direction, which is indeed the case in capillaries. Again, the coefficients a and b are quite complex and lengthy, however, the coefficients c and e may be found by evaluating the integrations. They take the forms

$$\begin{aligned} c \quad &= \frac{A^2\sin(2Bh) + 8AC\cos(Bh) - (4BC^2 + 2A^2B)h}{4B} \\ &\quad - \frac{A^2\sin(2BH) + 8AC\cos(BH) - (4BC^2 + 2A^2B)H}{4B}, \end{aligned} \tag{7.3}$$

$$e = \frac{2AC}{B} - \frac{A^2\sin(2Bh) + 8AC\cos(Bh) - (4BC^2 + 2A^2B)h}{4B}. \tag{7.4}$$

The interesting thing about this scenario stems from the fact that it mimics, to some extent, a tortious path, which fluids usually encounter in porous medium flows. Therefore, it would be interesting to explore this scenario in order to investigate how the meniscus will behave in such cases. In all the considered scenarios, the following parameters are set constant

$r_{p,min}$, m	5×10^{-5}	$r_{p,max}$, m	1×10^{-4}	μ_1 (Pa s)	1×10^{-5}	μ_2 (Pa s)	1×10^{-3}
H (m)	1.0	ϑ	45°	γ (N m^{-1})	0.072	λ	100

The parameter that is set free is the wavenumber, $\kappa = H/\varepsilon$, which determines the number of full cycles along the tube length. In this work, the values of κ that are considered include 0, 3, 4 and 5, with the value of 0 representing the case of a straight tube. The angle of tangency (α) of the tube profile is $\alpha = \tan^{-1}(\mathrm{d}r_p/\mathrm{d}z)$, with $\mathrm{d}r_p/\mathrm{d}z = AB\cos(Bz)$.

The normalized location of the meniscus is plotted against normalized time for the different scenarios and is shown in figure 20 for different wavenumbers. In addition, two cases of straight tubes with radii equal to $r_{p,min}$ and $r_{p,max}$, are also considered. It is clear that the profiles of the location of the meniscus of all the considered scenarios are set between the two straight cases. Furthermore, they feature a wavy nature as a consequence of the sinusoidal profile of the tube with number of cycles in accordance with that of the tube.

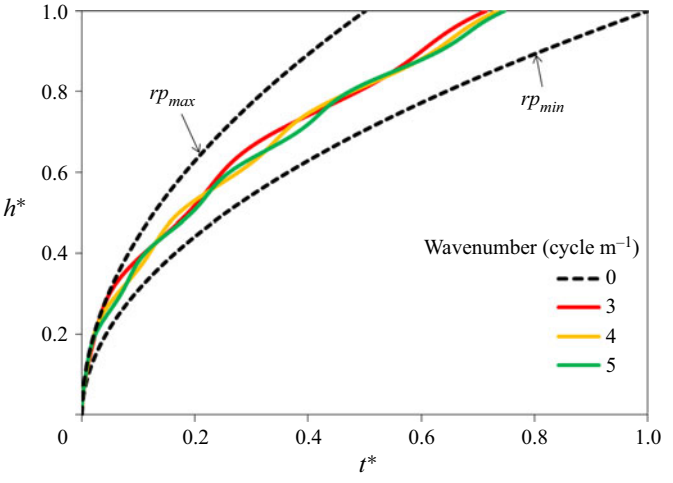

Figure 20. The normalized location of the meniscus with normalized times for different wavenumbers. In addition, two scenarios of straight tubes with the same maximum and minimum radii are also shown.

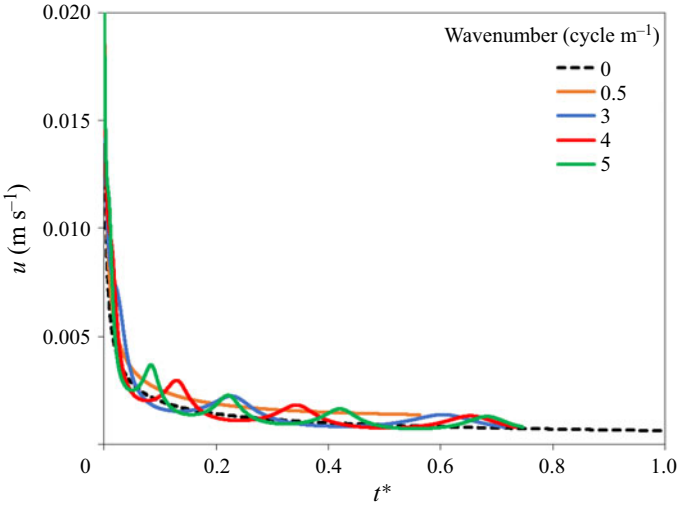

Figure 21. Velocity profile for the case of a sinusoidal tube profile with different cycles along the length of the tube on a linear scale.

Such a wavy nature of the location of the meniscus implies a similar wavy pattern for the speed of the meniscus as depicted in figure 21 (on a linear scale) and figure 22 (on logarithmic scale). From figure 21, it is clear that the speed of the meniscus generally decreases along the tube length. Furthermore, the period of change of the speed along the tube also changes with time (being longer at later time), which is a manifestation of the decrease in the average speed with time.

8. Imbibition against gravity

When gravity is involved, which corresponds to the case of a vertically, upward-oriented capillary tube, if the tube is long, an interesting possibility arises. This is when the

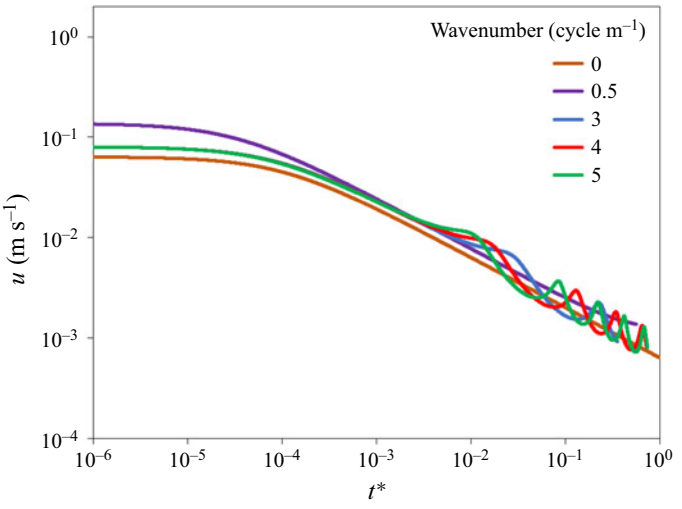

Figure 22. Velocity profiles for different wavenumbers in cycles/m over a logarithmic scale.

capillary force is balanced by the gravitational force and the interface ceases to climb upwards at a particular height, called the equilibrium height. While it is relatively simple to estimate this height in straight capillaries, it is not that straightforward when the radius of the tube changes along its length. In this case, the radius of curvature of the interface is a function of the profile of the tube, i.e. $r_p = r_p(h)$. When gravity is present, a nonlinear equation may be developed for the equilibrium height, the roots of which determine such a height. The equation that governs imbibition in which gravity exists may be written as

$$-[8\mu_1 r_p^2(h)(a + b\lambda)]\frac{\mathrm{d}h}{\mathrm{d}t} - \rho_1 g(c + e\xi) + 2r_p(h)\gamma\cos(\theta - \alpha) = 0. \tag{8.1}$$

When the meniscus has reached its terminal location, it is obvious that its speed becomes zero, or $\mathrm{d}h/\mathrm{d}t = 0$. Substitution into the above equation yields

$$\rho_1 g[c(h) + \xi e(h)] = 2r_p(h)\gamma\cos[\theta - \alpha(h)]. \tag{8.2}$$

On rearrangement, one obtains

$$r_p(h) = \frac{\rho_1 g[c(h) + \xi e(h)]}{2\gamma\cos[\theta + \alpha(h)]}. \tag{8.3}$$

The integral parameters c and e are geometrical factors that depend on the profile of the tube and are, therefore, functions of h. For the case of a linearly varying converging/diverging capillary tube, we have $r_p(h) = r_p(0) + mh$. Substitution yields the following relationship for the equilibrium height:

$$h = \frac{\rho_1 g(c + e\xi)}{2\gamma m\cos(\theta + \alpha)} - \frac{r_p(0)}{m}. \tag{8.4}$$

Let $\Lambda = \rho_1 g/2\gamma\cos(\theta + \alpha)$, then the above equation reduces to

$$mh = \Lambda(c + e\xi) - r_p(0). \tag{8.5}$$

On rearrangement, we get the following nonlinear equation for the terminal height in the form $f(h) = \text{const.}$, or:

$$f(h) = \Lambda[c(h) + \xi e(h)] - mh = r_p(0). \tag{8.6}$$

The parameters $c(h)$, and $e(h)$ are as given in table 1. The admissible root of the above equation determines the terminal location of the meniscus. One may observe that, for a diverging straight tube (i.e. $m > 0$), the larger the value of m, the smaller h will be. Conversely, for a converging tube (i.e. $m < 0$), the larger the value of m, the larger h will be. For the sake of illustration, let us consider the following examples of a converging and a diverging linear straight tube scenario. The first case represents a diverging capillary tube with $r_p(H)/r_p(0) = 10$. Parameters used for the example of a capillary rise in a diverging tube with a diameter ratio of 10 are listed below.

$r_p(0)$ (m)	1.0×10^{-4}	$r_p(H)$ (m)	1.0×10^{-3}	H (m)	1.0	γ (N m^{-1})	0.072
ϑ	45°	α	0.05°	ρ_1 (kg m^{-3})	1.0	ρ_2 (kg m^{-3})	1000
ξ	1000	μ_1 (Pa s)	1.0×10^{-5}	μ_2 (Pa s)	1.0×10^{-3}	λ	100

Implementing these parameters into (8.6), one may be able to find the value of the equilibrium height, h. A graphical implementation of the above equation is shown in figure 23. The function in (8.6) is modified by dividing through by m. It takes the form $f(h) = (\Lambda/m)[c(h) + \xi e(h)] - h$, and the right-hand side is $r_p(0)/m$. For a diverging scenario, the parameters used are those listed above. For the converging scenario, the parameters are the same except that the radius ratio $r_p(H)/r_p(0)$ is 0.1, with both having the same $r_p(0)$. The intersection of $f(h)$ and the constant $r_p(0)/m$ define the location of the meniscus at equilibrium. Furthermore, the two cases were also investigated using the developed model and were solved numerically, as given previously, and an almost exact match is obtained. Figure 24(*a*) shows the profiles depicting the location and the speed of the meniscus with time for the diverging scenario. As is clear, the location of the meniscus asymptotically approaches an equilibrium height of 0.075 m. This conforms to that theoretically derived, as depicted in figure 23(*b*). For a converging capillary, on the other hand, the location of the meniscus is found to be approximately 0.103 m, as obtained using both the developed general model and the analytical one (figure 23*c*,*d*).

For the sake of comparison, it is interesting to examine the location of the meniscus at equilibrium for a straight tube with the same $r_p(0)$. Using the formula $h = 2\gamma \cos\vartheta/r_{p0}\rho g$, one finds that $h = 0.104$ m, which is larger than those for converging and diverging scenarios.

To enlarge the scope of the comparisons with respect to the ratio between the equilibrium height of a straight capillary tube with that of converging/diverging ones of arbitrary radius ratio, an analysis of this topic is highlighted in this section. For simplicity, let us focus our attention to the case of spontaneous imbibition, where the displaced fluid is a gas. It is known that, at equilibrium, both the gravity and capillary forces balance each other. Analysis in Appendix C shows that

$$\frac{h_{C/D}}{h_S} = \frac{3\cos(\vartheta + \alpha)/\cos\vartheta}{\left[\frac{r_{p0}}{r_{ph}} + \frac{r_{ph}}{r_{p0}} + 1\right]}, \tag{8.7}$$

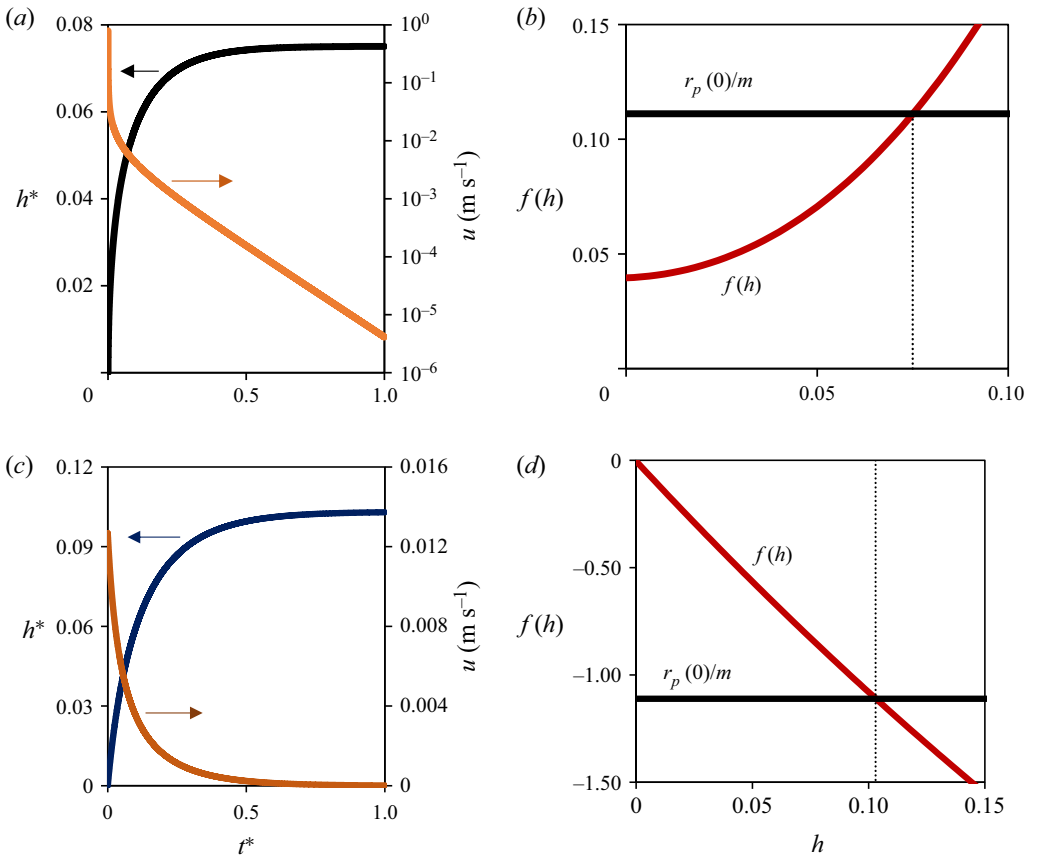

Figure 23. Equilibrium height for converging/diverging straight tubes, h^* is the normalized location of the meniscus and u is its speed. The intersection of the function $f(h)$, $[f(h) = (\Lambda/m)[c(h) + \xi e(h)] - h]$ and the line $r_p(0)/m$ defines the solution of (8.6), which determines the location of the meniscus. (*a*) Simulated equilibrium height (diverging straight tube). (*b*) Calculated equilibrium height (diverging straight tube). (*c*) Simulated equilibrium height (converging straight tube). (*d*) Calculated equilibrium height (diverging straight tube).

where $h_{C/D}$ is the equilibrium height of the meniscus in a converging/diverging capillary tube, h_S is the equilibrium height of the meniscus inside a straight tube with the same radius at the inlet, r_{p0} is the tube radius at the inlet, r_{ph} is the tube radius at the location of the meniscus and α is the angle of inclination of the converging/diverging tube. Derivation of the above equation is presented in Appendix C. For the case in which α is small, the above equation reduces to

$$\frac{h_{C/D}}{h_S} = \frac{3}{\left[\frac{r_{p0}}{r_{ph}} + \frac{r_{ph}}{r_{p0}} + 1\right]}. \tag{8.8}$$

Furthermore, when $r_{p0} = r_{ph}$ (i.e. straight tube), the above ratio is one. Equation (8.8) indicates that the equilibrium height for a converging/diverging straight tapered tube is always smaller than that of the corresponding straight tube with the same inlet radius. It is interesting to also explore the cases of converging/diverging and sinusoidal profiles for the cases of upward imbibition against gravity. Figure 24 shows the profiles of the location of

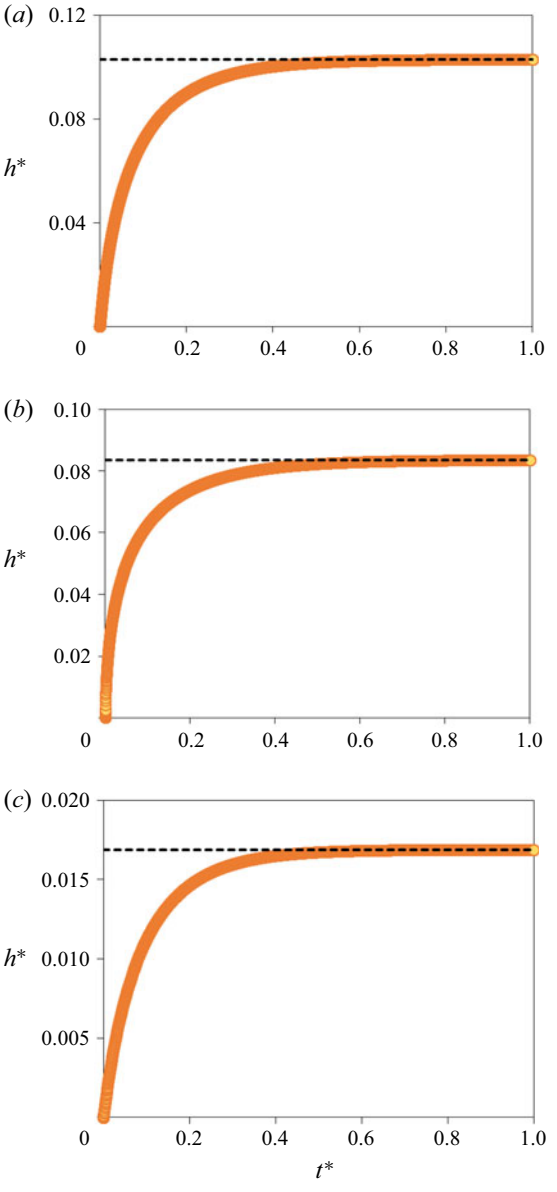

Figure 24. Imbibition in converging/diverging quadratic tube profiles (*a*,*b*) as well as in sinusoidal one (*c*) when gravity is considered. The profiles approach asymptotically the equilibrium height. (*a*) Converging quadratic tube: $H = 1.0$ m, $r_p(0) = 1.0 \times 10^{-4}$ m, $r_p(H) = 1.0 \times 10^{-5}$ m, $r_p(H)/r_p(0) = 0.1$, $\epsilon = [r_p(H) - r_p(0)]/H^2 = -0.00009$, $r_p(z) = 0.0001 - 0.00009z^2$. (*b*) Diverging quadratic tube: $H = 1.0$ m, $r_p(0) = 1.0 \times 10^{-4}$ m, $r_p(H) = 1.0 \times 10^{-3}$ m, $r_p(H)/r_p(0) = 10$, $\epsilon = [r_p(H) - r_p(0)]/H^2 = 0.0009$, $r_p(z) = 0.001 + 0.0009z^2$. (*c*) Sinusoidal profile: $H = 1.0$ m, $r_{p,min} = 1.0 \times 10^{-4}$ m, $r_{p,max} = 1.0 \times 10^{-3}$ m, $r_{p,max}/r_{p,min} = 10$, $n = \#\,Cycles = 5$.

the meniscus for the case of a converging/diverging quadratic and sinusoidal profiles, with the geometric parameters as given on the figures.

As one notices, the gravity equilibrates the interfacial force within the tube. This is manifested by noticing the profiles of the location of the meniscus, which show that they

reach a terminal location inside the tubes. For the case of a converging quadratic tube with parameters as given in figure 24(*a*), the meniscus rises to a height of approximately 0.103 m, which is slightly smaller than that of a straight tube of the same $r_p(0)$. For the case of a diverging quadratic profile with parameters as given in figure 24(*b*), the meniscus equilibrates at a height of 0.0835 m. Lastly, for the case of sinusoidal profile (figure 24*c*), the meniscus equilibrates at a height of 0.017 m. In other words, the equilibrium height for all the considered profiles is smaller than that of a straight tube having the same inlet radius. Finally, the model, as developed, can be implemented in studying two-phase flows in porous media (El Amin, Salama & Sun 2011) as well as in dynamic pore network models to locate the meniscus as it develops in the pore throats. It can also be used in the modelling of the filtration of emulsions using polymeric-type membranes (Salama, Zoubeik & Henni 2017; Zoubeik, Salama & Henni 2018; Echakouri, Salama & Henni 2020)

9. Conclusion

In this work, a model is developed to investigate imbibition/drainage processes in capillaries with arbitrary axisymmetric cross-sections. It generalizes previous models and accounts for, pressure, gravity, capillary and friction forces. While the model is derived to be general, the effects of inertia have been neglected in the considered scenarios. Furthermore, the model does not account for electrostatic forces that may arise due the accumulation of charges, particularly in nanosized tubes. The model lumps all the complexities of the fluids, the geometry and the contrast in properties into a single nonlinear differential equation with the primary variables including the location of the meniscus and its speed. Three scenarios of tube profiles are considered including, tapered straight tubes, quadratically varying tubes and sinusoidal ones. In all these scenarios, the tube profile maintains a small angle of tangency (i.e. $|\mathrm{d}r_p/\mathrm{d}z| \ll 1$). The developed model reduces to that recently developed for straight capillaries. It also reduces to the Washburn–Lucas model for spontaneous imbibition in horizontal capillaries. A fourth-order accurate, Runge–Kutta scheme has been assimilated to solve the model's equation. In addition, an analytical expression has been developed for the case of converging/diverging straight horizontal tubes. The numerical algorithm shows perfect match with the analytical solution.

The cases of spontaneous imbibition in horizontal capillaries of axially varying cross-section have been investigated first. For a converging straight capillary tube, interesting patterns have been observed. Under the prescribed assumptions, when the radius ratio $r_p(0)/r_p(H)$ equals the viscosity ratio between the invading wetting fluid and the non-wetting one, the speed of the meniscus assumes a constant value and its location follows a linear path. This indicates that both the friction and capillary forces balance each other along the tube. If $r_p(0)/r_p(H) < \lambda$, the location of the meniscus follows a nonlinear path with a continuously decreasing slope, which implies a continuous decrease in the speed of the meniscus along the tube. This indicates that, in this regime, the friction force is larger than the capillary force. If, on the other hand, $r_p(0)/r_p(H) > \lambda$, the speed of the meniscus increases along the tube, indicating that, in this regime, the capillary force is larger than the overall friction force. Other scenarios including the case of a quadratically varying converging/diverging tube as well as sinusoidal ones have also been studied.

For a quadratically diverging tube profile, the meniscus advances first at a faster pace when the degree of divergence is large (i.e. larger r_{pH}/r_{p0}). This is due to the smaller overall resistance offered by the tube when r_{pH}/r_{p0} is large. Later, this trend reverses and the meniscus advances at a smaller pace when r_{pH}/r_{p0} is large because of the increase in

the cross-sectional area. Similar behaviour can be noticed for a quadratically converging tube, albeit opposite to the previous scenario. That is the meniscus advances at a slower rate compared with that of a straight tube having the same inlet diameter. This is due to the larger resistance offered by the tube, which is larger when r_{pH}/r_{p0} is smaller. Later in time, the meniscus advances at a faster rate in a nonlinear fashion over that for a straight tube of the same inlet tube radius, which is in accordance with the increase in the capillary pressure as the tube radius decreases.

For the case of a sinusoidal tube profile, the speed of the meniscus depends on the wavenumber for the same maximum and minimum radii. The wavenumber represents the number of complete cycles within the length of the tube, therefore, a tube with a wavenumber (κ) of 0.0 is a straight tube. The speed of the meniscus at the early time is larger when $\kappa > 0$ compared with the straight tube with a radius equal to the minimum radius. This is attributed to the larger resistance of the straight tube with the minimum radius compared with that of the sinusoidal profile. At a later time, the meniscus speed oscillates due to the periodic change in the tube radius.

Furthermore, the effect of gravity on the height at which the meniscus equilibrates for all the studied scenarios has also been investigated. The model shows the journey of the meniscus towards equilibrium. It can also be used to directly determine the equilibrium height. It has been identified that all the scenarios with the same radius of the tubes at the inlet result in the equilibrium height being smaller than that of a corresponding straight tube with the same inlet size.

The developed model is also able to investigate drainage scenarios in which a non-wetting fluid displaces a wetting one. In this case, a boosting pressure is needed to work against interfacial, friction and possibly gravity forces. If such a pressure force is enough to overcome these forces, the non-wetting fluid will be able to invade the capillary tube. The model can be used in pore dynamic network models to monitor the location of the meniscus (which is related to the saturation of the invading fluid) with time.

Declaration of interests. The author reports no conflict of interest.

Author ORCIDs.
Amgad Salama http://orcid.org/0000-0002-9073-5080.

Appendix A. Analytical expression for the dynamic location of meniscus in converging/diverging straight tubes

It has been established for converging/diverging straight tubes, that the speed of the meniscus may be calculated using

$$\frac{dh}{dt} = \frac{\gamma \cos(\theta + \alpha)/r_p(h)}{\left\{4\mu_1\left[\frac{1}{m(mh+\mathscr{b})} - \frac{1}{m(mH+\mathscr{b})} + \left(\frac{1}{m\mathscr{b}} - \frac{1}{m(mh+\mathscr{b})}\right)\lambda\right]\right\}} \tag{A1}$$

With some manipulations, the above equation simplifies to

$$\frac{\mathrm{d}h}{\mathrm{d}t} = \frac{\gamma \cos(\theta + \alpha)}{\left\{\frac{4\mu_1 H}{r_p(0)}\left[\frac{r_p(0)}{r_p(H)}\left(1 - \frac{h}{H}\right) + \left(\frac{h}{H}\right)\lambda\right]\right\}}. \tag{A2}$$

Let $\beta = r_p(0)/r_p(H)$, then substitution yields

$$\frac{\mathrm{d}h}{\mathrm{d}t} = \frac{\gamma \cos(\theta + \alpha)}{\left\{\frac{4\mu_1 H}{r_p(0)}\left[\beta\left(1 - \frac{h}{H}\right) + \left(\frac{h}{H}\right)\lambda\right]\right\}}. \tag{A3}$$

Simplifications and rearrangement yield

$$\frac{\mathrm{d}h}{\mathrm{d}t} = \frac{\gamma \cos(\theta + \alpha)}{\left\{\frac{4\mu_1 H}{r_p(0)}\left[(\lambda - \beta)\frac{h}{H} + \beta\right]\right\}}. \tag{A4}$$

For a diverging profile (i.e. $\beta < 1$), in cases when $\lambda \gg \beta$, the above equation reduces to

$$\frac{\mathrm{d}h}{\mathrm{d}t} = \frac{\gamma \cos(\theta + \alpha)}{\left\{\frac{4\mu_1 H}{r_p(0)}\left[\lambda\frac{h}{H} + \beta\right]\right\}}. \tag{A5}$$

Let $\psi = \gamma r_p(0)\cos(\theta + \alpha)/4\mu_1 H$, on substitution into (A4), one finds

$$\frac{\mathrm{d}h}{\mathrm{d}t} = \frac{\psi}{\left[(\lambda - \beta)\frac{h}{H} + \beta\right]}. \tag{A6}$$

Rearrangement and integration yield

$$\int_0^h \left[(\lambda - \beta)\frac{h}{H} + \beta\right]\mathrm{d}h = \int_0^t \psi\, \mathrm{d}t. \tag{A7}$$

The above equation yields

$$\frac{(\lambda - \beta)}{2H}h^2 + \beta h = \psi t. \tag{A8}$$

On rearrangement, one finds

$$\frac{(\lambda - \beta)}{2H\psi}h^2 + \frac{\beta}{\psi}h = t. \tag{A9}$$

The interesting scenario would be the case in which $\lambda = \beta$, and, in this case, the above equation becomes

$$\frac{\beta}{\psi}h = t. \tag{A10}$$

Which depicts a linear variation of h against t and also a constant speed of the meniscus along the tube.

Appendix B

In this appendix, we highlight the influence of the configuration of the tube on both capillary and friction forces. This discussion will be derived for the case of converging/diverging straight tubes, however, it is also applicable to other scenarios. In fact, one can gain more insight by reformatting (5.8) into a form that highlights the influence of both capillary and friction forces

$$\frac{\mathrm{d}h}{\mathrm{d}t} = \frac{\gamma r_p(h)\cos(\theta + \alpha)}{\{4\mu_1 r_p^2(h)[a(h) + b(h)\lambda]\}}. \tag{B1}$$

In this equation, the numerator, which represents the capillary force, is correlated with the geometrical factor, $r_p(h)$. Likewise, the denominator, which represents friction force, is proportional to $r_p^2(h)[a(h) + b(h)\lambda]$. One may normalize these parameters as follows:

(i) normalized numerator as $r_p(h)/r_p(0)$; and
(ii) normalized denominator as $r_p^2(h)[a(h) + b(h)\lambda]/r_p^2(0)(a + b)$;

where $a + b$ is a geometrical constant calculated as

$$a + b = \int_h^H \frac{\mathrm{d}z}{r_p^2(z)} + \int_0^h \frac{\mathrm{d}z}{r_p^2(z)} = \int_0^H \frac{\mathrm{d}z}{r_p^2(z)} = \text{const.} \tag{B2}$$

We investigate how these parameters change along the tube and how they influence the contribution of capillary and friction forces. Starting with a converging straight tube scenario with $r_p(0) = 0.001$ m, we consider four convergence cases; namely with $r_p(H)/r_p(0)$ equal to 0.5, 0.1, 0.01 and 0.001. We also consider a diverging scenario for which $r_p(0) = 0.0001$ m and $r_p(H)/r_p(0) = 10$. It is to be mentioned that the geometrical parameters a, and λb represent the contributions to the total resistance of the displaced and the displacing fluids, respectively.

Figure 25(a) shows the variations of the normalized geometrical parameters along the tube when $r_p(H)/r_p(0) = 0.5$ (i.e. for a converging straight tube). The parameter $\lambda b/(a + b)$, which represents the contribution of the invading fluid into the overall friction force, takes over the resistance early once the meniscus starts to move as shown in the left-hand side figure. On compiling this into the right-hand side figure, it is clear that on multiplication of these geometric parameters with the square of the radius of the tube at the location of the meniscus, the overall friction force still increases along the tube. On the other hand, the net the capillary force reduces along the tube because of the reduction in the tube diameter.

This implies that the meniscus experiences drag that leads to its speed continuing to decrease along the tube. For the case when $r_p(H)/r_p(0) = 0.1$, as shown in figure 25(b), the invading fluid takes over the resistance a little late. In other words, at the beginning, the resistance of the displaced fluid contributes the most to the overall resistance before the resistance of the invading fluid takes over, as shown in the left-hand side figure. The right-hand side figure shows the overall friction and capillary forces along the tube. It is interesting to notice that the friction force increases at the beginning until approximately half the tube length then decreases. This implies that, at the beginning, it is the parameter $(a + \lambda b)/(a + b)$ that contributes the most, before the radius of the tube takes over. In comparison with capillary force, the friction force is still larger (as shown in the right-hand side figure), and, therefore, the meniscus decelerates.

For the case when $r_p(H)/r_p(0) = 0.01$, interesting features are observed. First of all, the influence of the resistance of the invading fluid becomes important later towards the middle of the tube. In other words, it is the resistance of the displaced fluid that dominates the overall resistance at the start, as depicted in figure 25(c) (left-hand side). The effect of the radius of the tube is interesting for this particular scenario. As shown in figure 25(c) (right-hand side), the friction force drops linearly along the tube, coinciding with that of the capillary force. This implies that, in this particular scenario, the meniscus moves at a constant speed.

Further decrease in radius ratio, likewise, shows interesting features. As shown in figure 25(d) (left-hand side), for the scenario $r_p(H)/r_p(0) = 0.001$, the contribution of the displaced fluid to the friction force dominates the overall friction, except towards the end of the tube. The effect of the radius of the tube along its length is shown in figure 25(d) (right-hand side). It is interesting to notice that the friction force is smaller than the capillary force and hence there is an increase in the speed of the meniscus along the tube.

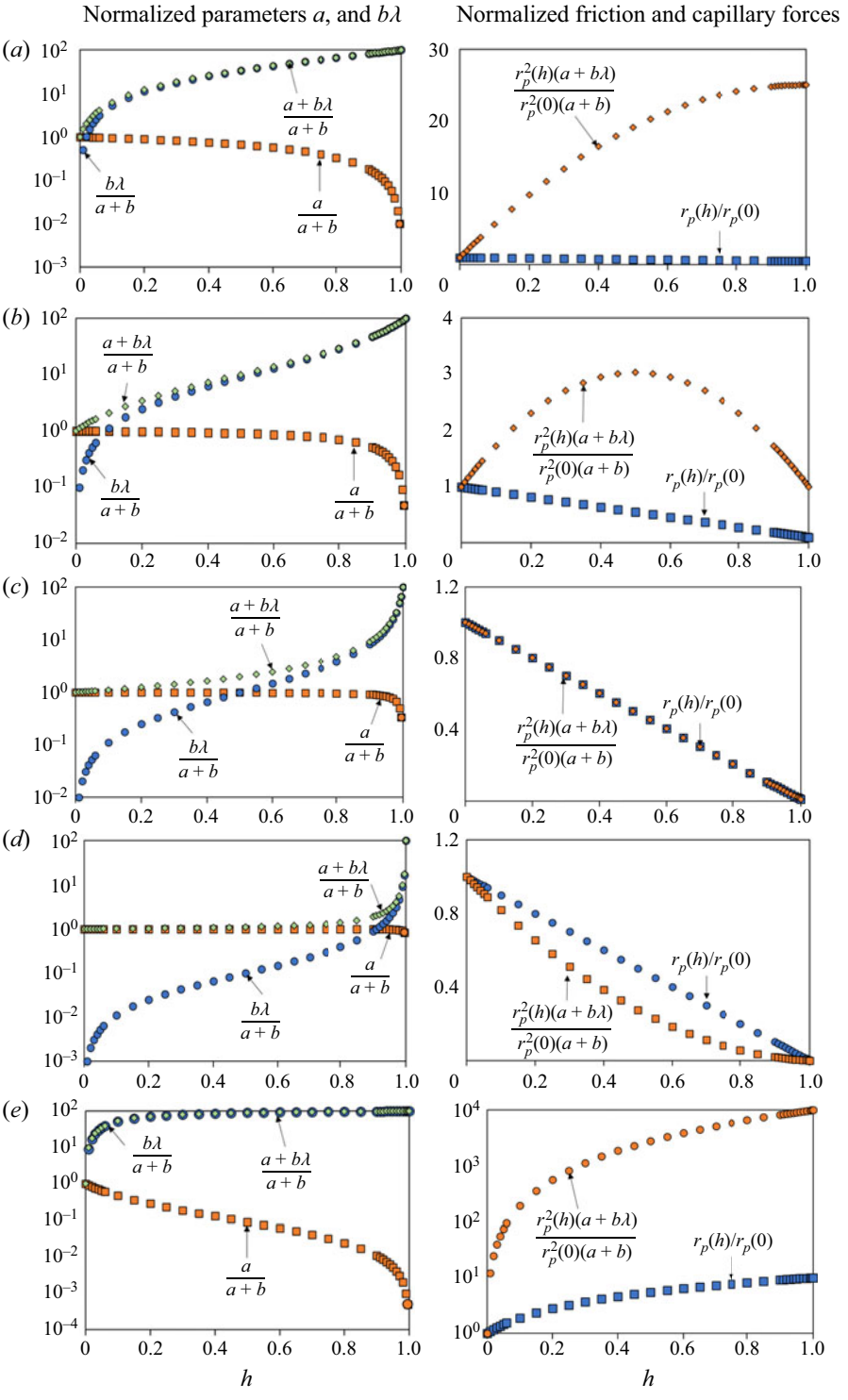

Figure 25. Variations of the geometric parameters a, and b (left-hand side) and of the friction and capillary parameters (right-hand side) along the tube length. (*a*) $r_p(H)/r_p(0) = 0.5$, $r_p(0) = 0.001$ m; (*b*) $r_p(H)/r_p(0) = 0.1$, $r_p(0) = 0.001$ m; (*c*) $r_p(H)/r_p(0) = 0.01$, $r_p(0) = 0.001$ m; (*d*) $r_p(H)/r_p(0) = 0.001$, $r_p(0) = 0.001$ m; (*e*) $r_p(H)/r_p(0) = 10$, $r_p(0) = 10 - 4$ m.

The case of a diverging capillary tube, on the other hand, for one radius ratio ($r_p(H)/r_p(0) = 10$) is shown in figure 25(*e*). As seen on the left-hand side figure, the friction force due to the invading fluid dominates the overall friction force right from the beginning and this leads the friction force always dominating the capillary force and the speed of the meniscus always decreasing.

Appendix C. Equilibrium height in converging/diverging capillaries

When an invading wetting fluid imbibes into a vertical tube that is filled initially with a non-wetting fluid, it rises against the gravity by the virtue of interfacial forces. When the tube is converging or diverging along its length, it is interesting to determine that height along the tube where the meniscus equilibrates (i.e. stop moving upwards). The invading fluid in the converging/diverging tube represents a truncated cone whose volume may be determined as

$$V = \tfrac{1}{3}\pi h[r_{po}^2 + r_{ph}^2 + r_{p0}r_{ph}], \tag{C1}$$

where V is the volume of the invading fluid, r_{po} is the radius at the start of the tube and r_{ph} is the radius of the tube at a height h where the meniscus exists. Gravitational force over the column of the invading fluid is $\rho g V = \pi h \rho g[r_{po}^2 + r_{ph}^2 + r_{p0}r_{ph}]/3$, and the capillary force is $2\pi r_{ph}\gamma\cos(\vartheta + \alpha)$, where $\alpha < 0$ for a converging tube and is $\alpha > 0$ for a diverging one. Equating the two forces yields

$$2\pi r_{ph}\gamma\cos(\vartheta + \alpha) = \tfrac{1}{3}\pi h\rho g[r_{po}^2 + r_{ph}^2 + r_{p0}r_{ph}]. \tag{C2}$$

From which one can determine the height of the meniscus $h_{C/D}$, as

$$h_{C/D} = \frac{6r_{ph}\gamma\cos(\vartheta + \alpha)}{\rho g[r_{po}^2 + r_{ph}^2 + r_{p0}r_{ph}]}. \tag{C3}$$

For a uniform straight tube, the equilibrium height (h_S) of the meniscus in a tube with the same radius at the beginning (i.e. same r_{p0}) may be determined as

$$h_S = \frac{2\gamma\cos\vartheta}{r_{p0}\rho g}. \tag{C4}$$

With some simplifications, the ratio between $h_{C/D}$ and h_S is

$$\frac{h_{C/D}}{h_S} = \frac{3\cos(\vartheta + \alpha)/\cos\vartheta}{\left[\frac{r_{p0}}{r_{ph}} + \frac{r_{ph}}{r_{p0}} + 1\right]}. \tag{C5}$$

For small α

$$\frac{h_{C/D}}{h_S} = \frac{3}{\left[\frac{r_{p0}}{r_{ph}} + \frac{r_{ph}}{r_{p0}} + 1\right]}. \tag{C6}$$

According to the above equation, when $r_{ph} = r_{p0}$, it is clear that $h_{C/D} = h_S$. For any other ratio, one finds $h_{C/D} < h_S$.

References

Ashraf, S. & Phirani, J. 2019*a* A generalized model for spontaneous imbibition in a horizontal, multi-layered porous medium. *Chem. Engng Sci* **209**, 115175.

Ashraf, S. & Phirani, J. 2019*b* Capillary displacement of viscous liquids in a multi-layered porous medium. *Soft Matter* **15**, 2057–2070.

Ashraf, S., Visavale, G. & Phirani, J. 2018 Spontaneous imbibition in randomly arranged interacting capillaries. *Chem. Engng Sci.* **192**, 218–234.

Bashtani, F., Irani, M. & Kantzas, A. 2021 Scale up of pore-network models into reservoir scale: optimization of inflow control devices placement. *SPE J.* **1-18**, SPE-208601-PA.

Bijeljic, B., Markicevic, B. & Navaz, H.K. 2011 Capillary climb dynamics in the limits of prevailing capillary and gravity force. *Phys. Rev.* E **83**, 056310.

Budaraju, A., Phirani, J., Kondaraju, S. & Bahga, S.S. 2016 Capillary Displacement of Viscous Liquids in Geometries with Axial Variations. *Langmuir* **32** (41), 10513–10521.

Bultreys, T., Van Hoorebeke, L. & Cnudde, V. 2015 Multi-scale, micro-computed tomography-based pore network models to simulate drainage in heterogeneous rocks. *Adv. Water Resour.* **78**, 36–49.

Clift, R., Grace, J.R. & Weber, M.E. 2005 *Bubbles, Drops, and Particles*, 1st edn. Dover.

Das, D.B. & Hassanizadeh, S.M. 2010 *Upscaling Multiphase Flow in Porous Media: From Pore to Core and Beyond*. Springer.

Das, S., Chanda, S., Eijkel, J.C.T., Tas, N.R., Chakraborty, S. & Mitra, S.K. 2014 Filling of charged cylindrical capillaries. *Phys. Rev.* E **90**, 043011.

Das, S., Guha, A. & Mitra, S.K. 2013 Exploring new scaling regimes for streaming potential and electroviscous effects in a nanocapillary with overlapping electric double layers. *Anal. Chim. Acta* **804**, 159–166.

Das, S. & Mitra, S.K. 2013 Different regimes in vertical capillary filling. *Phys. Rev.* E **87** (6), 063005.

Das, S., Waghmare, P.R. & Mitra, S.K. 2012 Early regimes of capillary filling. *Phys. Rev.* E **86** (6), 067301.

de Boer, R. 2006 *Trends in Continuum Mechanics of Porous Media*. Springer.

de Gennes, P., Brochard-Wyart, F. & Quere, D. 2004 *Capillarity and Wetting Phenomena: Drops, Bubbles, Pearls, Waves*. Springer.

Dereyssat, M., Courbin, L., Reyssat, E. & Stone, H. 2008 Imbibition in geometries with axial variations. *J. Fluid Mech.* **615**, 335–344.

Echakouri, M., Salama, A. & Henni, A. 2020 Experimental and computational fluid dynamics investigation of the deterioration of the rejection capacity of the membranes used in the filtration of oily water systems. *ACS ES&T Water* **1** (3), 728–744.

El Amin, M., Salama, A. & Sun, S. 2011 Solute transport with chemical reaction in single and multi-phase flow in porous media. In *Mass Transfer in Multiphase Systems and its Applications* (ed. M. El-Amin). IntechOpen. doi:10.5772/594.

Elizalde, E., Urteaga, R., Koropecki, R.R. & Berli, C.L.A. 2014 Inverse problem of capillary filling. *Phys. Rev. Lett.* **112**, 134502.

Erickson, D., Li, D. & Park, C.B. 2002 Numerical simulations of capillary-driven flows in nonuniform cross-sectional capillaries. *J. Colloid Interface Sci.* **250**, 422–430.

Fries, N. & Dreyer, M. 2008 The transition from inertial to viscous flow in capillary rise. *J. Colloid. Interface Sci.* **327**, 125–128.

Golparvar, A., Zhou, Y., Wu, K., Ma, J. & Yu, Z. 2018 A comprehensive review of pore scale modeling methodologies for multiphase flow in porous media. *Adv. Geo-Energy Res.* **2** (4), 418–440.

Gorce, J.-B., Hewitt, I. & Vella, D. 2016 Capillary imbibition into converging tubes: beating Washburn's law and the optimal imbibition of liquids. *Langmuir* **32** (6), 1560–1567.

Gueto-Felgueroso, L., Fu, X. & Juanes, R. 2018 Pore-scale modeling of phase change in porous media. *Phys. Rev. Fluids* **3**, 084302.

Guo, Y., Zhang, L., Sun, H., Yang, Y., Xu, Z., Bao, B. & Yao, J. 2021 The simulation of liquid flow in the pore network model of nanoporous media. ASME. *J. Energy Resour. Technol.* **143** (3), 033006.

Hammecker, C., Mertz, J.-D., Fischer, C. & Jeannette, D. 1993 A geometrical model for numerical simulation of capillary imbibition in sedimentary rocks. *Transp. Porous Media* **12**, 125–141.

Hultmark, M., Aristoff, J.M. & Stone, H.A.J. 2011 The influence of the gas phase on liquid imbibition in capillary tubes. *Fluid Mech* **678**, 600–606.

Joekar-Niasar, V., Prodanovic, M., Wildenschild, D. & Hassanezadeh, S.M. 2010 Network model investigation of interfacial area, capillary pressure and saturation relationships in granular porous media. *Water Resour. Res.* **46**, W06526.

KORNEV, K.G. & NEIMARK, A.V. 2011 Spontaneous penetration of liquids into capillaries and porous membranes revisited. *J. Colloid. Interface Sci.* **235** (1), 101–113.

LIOU, W.W., PENG, P. & PARKER, P.E. 2009 Analytical modeling of capillary flow in tubes of nonuniform cross section. *J. Coll. Interface Sci.* **333** (1), 389–399.

LUCAS, R. 1918 Rate of capillary ascension of liquids. *Kolloidn. Z.* **23** (15), 15–22.

MAGGI, F. & ALONSO-MARROQUIN, F. 2012 Multiphase capillary flows. *Intl J. Multiphase Flow* **42**, 62–73.

OVAYSI, S. & PIRI, M. 2011 Pore-scale modeling of dispersion in disordered porous media. *J. Contam. Hydrol.* **124** (1–4), 68–81.

RAEINI, A.Q., BLUNT, M.J. & BIJELJIC, B. 2012 Modelling two-phase flow in porous media at the pore scale using the volume-of-fluid method. *J. Comput. Phys.* **231** (17), 5653–5668.

RAMAKRISHNAN, S., WU, P., ZHANG, H. & WASAN, D.T. 2019 Dynamics in closed and open capillaries. *J. Fluid Mech.* **872**, 5–38.

REYSSAT, E. 2014 Drops and bubbles in wedges. *J. Fluid Mech.* **748**, 641–662.

SALAMA, A. 2021*a* Imbibition and drainage processes in capillaries: a generalized model, effect of inertia, and a numerical algorithm. *Phys. Fluids* **33** (8), 082104.

SALAMA, A. 2021*b* A generalized analytical model for estimating the rate of imbibition/drainage of wetting/nonwetting fluids in capillaries. *Chem. Engng Sci.* **243**, 116788.

SALAMA, A., CAI, J., KOU, J., SUN, S., EL AMIN, M.F. & WANG, Y. 2021 Investigation of the dynamics of immiscible displacement of a ganglion in capillaries. *Capillarity* **4** (2), 31–44.

SALAMA, A., KOU, J., ALYAN, A. & HUSEIN, M.M. 2022 Capillary-driven ejection of a droplet from a micropore into a channel: a theoretical model and a computational fluid dynamics verification. *Langmuir* **38** (14), 4461–4472.

SALAMA, A. & VAN GEEL, P.J. 2008 flow and solute transport in saturated porous media I: the continuum hypothesis. *Porous Media* **11** (4), 403–413.

SALAMA, A., ZOUBEIK, M. & HENNI, A. 2017 A multicontinuum approach for the problem of filtration of oily water systems across thin flat membranes: I. The framework. *AIChE J.* **63** (10), 4604–4615.

TARONI, M. & VELLA, D. 2012 Multiple equilibria in a simple elastocapillary system. *J. Fluid Mech.* **712**, 273–294.

WAGHMARE, R. & MITTRA, S.K. 2010 Finite reservoir effect on capillary flow of microbead suspension in rectangular microchannels. *J. Colloid. Interface Sci.* **351** (2), 561–569.

WALLS, P.L.L., DEQIDT, G. & BIRD, J.C. 2016 Capillary displacement of viscous liquids. *Langmuir* **32** (13), 3186–3190.

WANG, Z., CHANG, C.-C., HONG, S.-J., SHENG, Y.-J. & TSAO, H.-K. 2012 Capillary rise in a microchannel of arbitrary shape and wettability: hysteresis loop. *Langmuir* **28** (49), 16917–16926.

WASHBURN, E.W. 1921 The dynamics of capillary flow. *Phys. Rev.* **17** (3), 273.

WHITTAKER, S. 1999 *The Method of Volume Averaging*. Springer.

XIAO, Y., YANG, F. & PITCHUMANI, R. 2006 A generalized analysis of capillary flows in channels. *J. Colloid. Interface Sci.* **298** (2), 880–888.

YOUNG, W.B. 2004 Analysis of capillary flows in non-uniform cross-sectional capillaries. *Colloids Surf.* A **234**, 123–128.

ZOUBEIK, M., SALAMA, A. & HENNI, A. 2018 A novel antifouling technique for the crossflow filtration using porous membranes: Experimental and CFD investigations of the periodic feed pressure technique. *Water Res.* **146**, 159–176.